Mon. Not. R. Astron. Soc. **396,** 964–983 (2009) doi:10.1111/j.1365-2966.2009.14756.x

Triggered star formation and evolution of T-Tauri stars in and around bright-rimmed clouds

Neelam Chauhan,[1] A. K. Pandey,[1★] K. Ogura,[2] D. K. Ojha,[3] B. C. Bhatt,[4] S. K. Ghosh[3] and P. S. Rawat[5]

[1]*Aryabhatta Research Institute of Observational Sciences (ARIES), Nainital 263 129, India*
[2]*Kokugakuin University, Higashi, Shibuya-ku, Tokyo 150-8440, Japan*
[3]*Tata Institute of Fundamental Research, Mumbai 400 005, India*
[4]*CREST, Indian Institute of Astrophysics, Hosakote 562 114, India*
[5]*Physics Department, D.S.B. Campus, Kumaun University, Nainital 263 002, India*

Accepted 2009 March 9. Received 2009 March 6; in original form 2008 July 12

ABSTRACT

The aim of this paper is to quantitatively testify the '*small-scale sequential star formation*' hypothesis in and around bright-rimmed clouds (BRCs). As a continuation of the recent attempt by Ogura et al., we have carried out BVI_c photometry of four more BRC aggregates along with deeper re-observations of two previously observed BRCs. Again, quantitative age gradients are found in almost all the BRCs studied in the present work. Archival *Spitzer*/Infrared Array Camera data also support this result. The global distribution of near-infrared excess stars in each H II region studied here clearly shows evidence that a series of radiation-driven implosion processes proceeded in the past from near the central O star(s) towards the peripheries of the H II region. We found that in general weak-line T-Tauri stars (WTTSs) are somewhat older than classical T-Tauri stars (CTTSs). Also the fraction of CTTSs among the T-Tauri stars (TTSs) associated with the BRCs is found to decrease with age. These facts are in accordance with the recent conclusion by Bertout, Siess & Cabrit that CTTSs evolve into WTTSs. It seems that in general the equivalent width of Hα emission in TTSs associated with the BRCs decreases with age. The mass function (MF) of the aggregates associated with the BRCs of the morphological type 'A' seems to follow that found in young open clusters, whereas 'B/C'-type BRCs show significantly steeper MF.

Key words: stars: evolution – stars: formation – stars: pre-main-sequence – H II regions.

1 INTRODUCTION

It is believed that majority of the stars in the Galaxy form in clusters that may contain massive ($M \gtrsim 10\,M_\odot$) as well as low-mass stars. A massive star has strong impact on the evolution of its parental molecular cloud. As soon as O stars form their strong ultraviolet (UV) radiation photoionizes the surrounding gas and develops an expanding H II region, thus dispersing the remaining molecular cloud. However, the UV radiation can also induce triggering of the next generation star formation. This phenomenon is known as 'sequential star formation'. Observational evidence for this process is often inferred from the spatial distribution of young stars and subgroups of OB associations and their age distribution (see e.g. Samal et al. 2007; Sharma et al. 2007; Jose et al. 2008; Pandey et al. 2008).

One of the triggered star formation processes is known as the 'collect and collapse process', which was proposed by Elmegreen & Lada (1977). As an H II region expands the surrounding neutral material is collected between the ionization front and the shock front which precedes the former. With time, the layer gets massive and consequently becomes gravitationally unstable and collapses to form stars of the second generation, including massive stars. So, this process can repeat itself. Recent simulations of this process include Hosokawa & Inutsuka (2005, 2006) and Dale, Bonnell & Whitworth (2007). An observational signature of the process is the presence of a dense layer and massive condensations adjacent to an H II region (e.g. Deharveng et al. 2003).

Another process which has been frequently supported by numerical simulations as well as by observations is radiation-driven implosion (RDI) of a molecular cloud condensation. In this process, a pre-existing dense clump is exposed to the ionizing radiation from massive stars of the previous generation. The head part of the clump collapses due to the high pressure of the ionized gas and the self-gravity, which consequently leads to the formation of next generation stars. Detailed model calculations of the RDI process have been carried out by several authors (e.g. Bertoldi 1989;

★E-mail: pandey@aries.ernet.in

Lefloch & Lazareff 1995; Lefloch, Lazareff & Castets 1997; De Vries, Narayanan & Snell 2002; Kessel-Deynet & Burkert 2003; Miao et al. 2006). The signature of the RDI process is the anisotropic density distribution in a relatively small molecular cloud surrounded by a curved ionization/shock front (bright rim).

Bright-rimmed clouds (BRCs) are small molecular clouds located near the edges of evolved H II regions and show the above signature. So, they are considered to be good laboratories to study the physical processes involved in the RDI process. Actually a Submillimeter Common-User Bolometer Array (SCUBA) imaging survey of the submillimeter continuum emission from BRCs has revealed the presence of embedded cores (Thompson et al. 2004; Morgan et al. 2008). Morgan et al. (2004) have shown the presence of a ionized boundary layer (IBL) at the interface between the H II region and the BRC molecular cloud. They have also shown that many BRCs may be in a post-shocked state and ongoing star formation, which may be due to the interaction with the external ionizing radiation. Further, many BRCs are associated with the signposts of recent/ongoing star formation such as Herbig–Haro objects and Infrared Astronomical Satellite (IRAS) point sources of low temperature that meet the criteria of young stellar objects (YSOs). Sugitani, Fukui & Ogura (1991) (hereafter SFO91) and Sugitani & Ogura (1994) compiled catalogues of altogether 89 BRCs, associated with IRAS point sources for the Northern and Southern hemispheres, respectively. Subsequently, Sugitani, Tamura & Ogura (1995) carried out near-infrared (NIR) imaging of 44 BRCs and revealed that an elongated, small cluster or aggregate of YSOs which are aligned along the direction towards the ionizing star is often associated with them. These aggregates showed a tendency that 'redder' (presumably younger) stars tend to be located inside the BRCs, whereas relatively 'bluer' (presumably older) stars are found outside the clouds, suggesting an age gradient. Thus they advocated a hypothesis called '*small-scale sequential star formation*' (S^4F), i.e. the propagation of star formation along the axis of the BRCs as the ionization/shock front advances further and further into the molecular cloud. The Hα grism survey of 24 BRCs by Ogura, Sugitani & Pickles (2002) detected 460 Hα emission stars [possibly, T-Tauri stars (TTSs) or Herbig Ae/Be stars] and 12 Herbig–Haro objects in their vicinities. Again these Hα emission stars are found concentrated towards the head or just outside of the BRCs and aligned towards the exciting star(s) direction. Deep NIR photometry of BRC 14 by Matsuyanagi et al. (2006) revealed that three indicators of star formation, i.e. the fraction of YSOs among the sources, the amount of extinction and the NIR excesses of the YSOs, show a clear trend from outside to the inside of the rim indicating that the YSOs located near the rim are relatively younger than those located away from the rim. This result further strengthens the S^4F hypothesis.

The best way to quantitatively testify the hypothesis is to estimate the ages of the aggregate members and to compare them between different regions with respect to the bright rim. Ogura et al. (2007, hereafter Paper I) undertook BVI_c photometry of four BRC aggregates (BRCs 11NE, 12, 14 and 37) and showed that the stars inside or on the bright rim tend to have younger ages than those outside it, which is exactly what is expected from the S^4F hypothesis. The main aim of the present study is to further confirm it and to investigate the star formation scenario in/around the BRCs. We have extended BVI_c photometry to four more BRCs, namely BRCs 2, 13, 27 and 38. In addition to them, we have re-observed BRCs 11NE and 14 to obtain deeper data.

The information about the observations and archival data is given in Sections 2 and 3, respectively. Section 4 describes the BRCs studied in the present work. The procedure to estimate the membership, age and mass of the YSOs is described in Section 5. The star formation scenario, evolution of disc of TTSs and mass functions (MFs) in the BRC regions are studied in Sections 6, 7 and 8, respectively. In Section 9, the conclusions of the present study are summarized.

2 OBSERVATIONS AND DATA REDUCTIONS

BVI_c CCD observations of BRCs 2, 11NE, 13, 14 and 27 were carried out using the 2048 × 2048 pixel^2 CCD camera mounted on 2.0-m *Himalayan Chandra Telescope* (*HCT*) of the Indian Astronomical Observatory (IAO), Hanle, India on 2006 October 27 and 28. The instrument Himalaya Faint Object Spectrograph Camera (HFOSC) was used in the imaging mode. The details of the site, *HCT* and HFOSC can be found at the *HCT* website (http://www.crest.ernet.in). The sky at the time of observations was photometric with a seeing size [full width at half-maximum (FWHM)] of ∼1.5 arcsec. The observations of the BRCs 2, 13, 27 were standardized on same night by observing standard stars in the SA113 field (Landolt 1992). The observations of BRCs 11NE and 14 were transformed to the standard system by using the BVI_c magnitudes given in Paper I.

The BVI_c observations of BRC 38 were obtained by using 2048 × 2048 pixel^2 CCD camera mounted at f/13 Cassegrain focus of the 1.04-m Sampurnanand Telescope (ST) at Aryabhatta Research Institute of Observational Sciences (ARIES), Nainital, India. The details of the CCD camera can be found in our earlier paper (e.g. Jose et al. 2008; Pandey et al. 2008). To improve the signal-to-noise ratio (S/N), the observations were carried out in a binning mode of 2 × 2 pixel. During the observations the seeing was about 2.1 arcsec. SA98 field of Landolt (1992) was observed on 2006 October 26 to standardize the observations. The log of the *HCT* and ST observations is tabulated in Table 1. A number of bias and twilight flat frames were also taken during the observing runs.

The data analysis was carried out at ARIES, Nainital, India. The initial processing of the data frames was done using various tasks available under the IRAF data reduction software package. The photometric measurements of the stars were performed using DAOPHOT II software package (Stetson 1987). The point spread function (PSF) was obtained for each frame using several uncontaminated stars. Aperture photometry was carried out for the standard stars to estimate the atmospheric extinction and to calibrate the observations. The following transformation equations were used to calibrate the observations:

$$(B - V) = m_1(b - v) + c_1$$

$$(V - I_c) = m_2(v - i) + c_2$$

$$V = v + m_3(v - i) + c_3,$$

where *b, v, i* are the instrumental magnitudes corrected for the atmospheric extinctions, and B, V, I_c are the standard magnitudes; c_1, c_2, c_3 and m_1, m_2, m_3 are zero-point constants and colour coefficients, respectively. The values of the zero-point constants and the colour coefficients are given in Table 2.

The standard deviations of the standardization residuals, Δ, between the standard and transformed magnitudes and colours of the standard stars, are found to be $\Delta V = 0.006$, $\Delta(B - V) = 0.007$ and $\Delta(V - I_c) = 0.007$ for the *HCT* data, whereas for the ST observations these values are 0.001, 0.010 and 0.002, respectively. The photometric accuracies depend on the brightness of the stars, and the typical DAOPHOT errors in B, V and I_c bands at $V \sim 18$ are smaller than 0.01 mag. Near the limiting magnitude of V ∼ 21, which is

Table 1. Log of optical observations.

Region	Telescope	Filter; exposure time (s) × no. of frames	Date of observations
BRC 2	*HCT*, Hanle	B : 600 × 4; V : 300 × 4; I_c : 180 × 4	2006.10.27
BRC 11	*HCT*, Hanle	B : 600 × 4; V : 300 × 4; I_c : 180 × 4	2006.10.28
BRC 13	*HCT*, Hanle	B : 600 × 4; V : 300 × 4; I_c : 180 × 4	2006.10.27
BRC 14	*HCT*, Hanle	B : 600 × 4; V : 300 × 4; I_c : 180 × 4	2006.10.27
BRC 27	*HCT*, Hanle	B : 600 × 4; V : 300 × 4; I_c : 180 × 4	2006.10.28
BRC 38	ST, Nainital	B :1800 × 4; V : 300 × 8; I_c : 600 × 3	2006.10.26

Table 2. The zero-point constants, colour coefficients and extinction coefficients.

Parameters	*HCT*	ST
Zero-point constants		
c1	−0.344 ± 0.024	−0.305 ± 0.011
c2	0.101 ± 0.005	0.541 ± 0.009
c3	−0.799 ± 0.017	−3.394 ± 0.010
Colour coefficients		
m1	0.855 ± 0.017	0.981 ± 0.008
m2	1.063 ± 0.005	0.990 ± 0.011
m3	0.078 ± 0.015	0.031 ± 0.009
Extinction coefficients		
K_b	0.219 ± 0.009	0.301 ± 0.010
K_v	0.122 ± 0.007	0.199 ± 0.009
K_i	0.056 ± 0.008	0.088 ± 0.010

practically the same for *HCT* and ST, the DAOPHOT errors increase to 0.11, 0.05, 0.02 mag in the *B, V* and I_c bands, respectively. The *B, V* and I_c photometric data for the stars along with their positions, equivalent widths (EWs) and corresponding Two Micron All Sky Survey (2MASS) data are given in Table 3.

3 ARCHIVE DATA

3.1 Near-infrared data from 2MASS

NIR JHK_s data for the stars in the BRC regions have been obtained from the 2MASS Point Source Catalog (PSC) (Cutri et al. 2003). Sources having uncertainty ≤0.1 mag (S/N ≥ 10) in all the three bands were selected to ensure high-quality data. The JHK_s data were transformed from the 2MASS system to the California Institute of Technology (CIT) system using the relations given in the 2MASS website. For BRC 14, we have adopted the JHK_s data by Matsuyanagi et al. (2006), which were obtained with the infrared (IR) camera Simultaneous-color Infra Red Imager for Unbiased Survey mounted on the University of Hawaii 2.2-m telescope.

3.2 Mid-infrared data from *Spitzer*/IRAC

We have also used archived mid-infrared (MIR) data from Infrared Array Camera (IRAC) of the *Spitzer* telescope. We obtained basic calibrated data (BCD) using the software LEOPARD. Mosaicking was performed using the MOPEX (Mosaicker and Point Source Extractor) software provided by *Spitzer Science Center* (SSC). All of our mosaics were built at the native instrument resolution of 1.2 arcsec pixel^{-1} with the standard BCDs. We used the standard IRAF photometry routines in the *apphot* package to detect sources and perform aperture photometry in each IRAC band. The FWHM of every detection is measured and all detections with FWHM > 3.6 arcsec are considered resolved and removed. The detections are also examined visually in each band to remove non-stellar objects and false detections. The sources with photometric uncertainties ≤0.2 mag in each band were considered as good detections. The photometry was done using an aperture radius of 3.6 arcsec and the background estimation was done within a concentric sky annulus of the inner and outer radii of 3.6 and 8.4 arcsec, respectively. We adopted the zero-point magnitudes for the standard aperture radius (12 arcsec) and background annulus of (12–22.4 arcsec) of 19.67, 18.93, 16.85 and 17.39 in the 3.6, 4.5, 5.8 and 8.0 μm bands, respectively. Aperture corrections were made using the values described in the IRAC Data Handbook (Reach et al. 2006).

4 DESCRIPTION OF THE BRCS STUDIED

A brief description of BRCs studied is given below.

BRC 2. Sharpless 171 (= NGC 7822) is a large H II region associated with the Cepheus OB4 association (Yang & Fukui 1992). This region contains three BRCs, BRCs 1-3 (SFO91). A star cluster Be 59, containing nine O7-B3 stars, is located at the centre of the H II region. Recently, Pandey et al. (2008) have made photometric studies of Be 59 and its surrounding region in detail. The distance to the cluster was estimated to be 1.0 kpc. The age of these massive stars is found to be about 1–4 Myr with an average of ∼2 Myr. It was also found that the stars around BRC 1, which is located about 3 pc towards west of Be 59, are younger than those in the cluster. This seems to support triggered star formation in the BRC 1 region due to the massive stars in Be 59.

BRC 2 is located about 17 pc north of Be 59. On the basis of MIR observations by IRAC of the *Spitzer Space Telescope*, Megeath et al. (2004) have reported a cluster of young stars near the edge of BRC 2. The distribution of YSOs suggests that their formation is triggered by a photoevaporation-driven shock propagating into the BRC 2 cloud.

BRCs 11NE, 13 and 14. The large H II region IC 1848 = S199, associated with the radio source W5, is located in the Perseus arm at the distance of about 1.9 kpc (SFO91). In fact, it is composed of two adjacent H II regions, namely IC 1848W and IC 1848E (Vallee, Hughes & Viner 1979; Karr & Martin 2003; Koenig et al. 2008). IC 1848W is ionized by HD 17505 (O6V) and HD 17520 (O9V), whereas IC 1848E is ionized by HD 18326 (O7V). The former harbours a young cluster (age ∼1 Myr; Feinstein, Vazquez & Benvenuto 1986). Carpenter, Heyer & Snell (2000) reported several deeply embedded star-forming sites in the W3/W4/W5 region and put forward the notion of triggered star formation in this complex. Based on a multiwavelength study of the W5 star-forming region, Karr & Martin (2003) investigated the star formation scenario and supported triggered star formation in this region.

SFO91 list four BRCs, BRCs 11–14 around IC 1848. BRC 11 is situated near the southern edge of IC 1848W, BRC 12 near its northern edge and BRCs 13 and 14 at the eastern edge of IC 1848E. There are two more BRCs in the vicinity of BRC11, which are

Table 3. *B*, *V* and I_c photometric data for the stars along with their positions, EWs and corresponding 2MASS data.

S. no.	RA (2000)	Dec. (2000)	$B \pm eB$ (mag)	$V \pm eV$ (mag)	$I_c \pm eI_c$ (mag)	EW [Hα] (Å)	2MASS name	J ± eJ (mag)	$H \pm eH$ (mag)	K ± eK (mag)	Q flag	C flag	ID(Ogura et al. 2002)
BRC 2													
1	00 03 57.1	+68 33 46.4	20.087 ± 0.009	18.049 ± 0.003	15.136 ± 0.004	16.3	00035705+6833465	13.067 ± 0.026	11.906 ± 0.031	11.220 ± 0.021	AAA	000	5
2	00 03 57.3	+68 33 23.0		22.450 ± 0.044	17.832 ± 0.004	274.4	00035728+6833229	14.863 ± 0.036	13.768 ± 0.035	13.174 ± 0.033	AAA	000	6
3	00 03 59.1	+68 32 47.4		21.134 ± 0.014	17.133 ± 0.005	28.1	00035905+6832472	14.681 ± 0.035	13.804 ± 0.042	13.315 ± 0.037	AAA	000	8
4	00 04 01.6	+68 34 14.2		17.975 ± 0.037	15.649 ± 0.014	2.7	00040165+6834137	13.737 ± 0.040	12.834 ± 0.037	12.447 ± 0.029	AAA	ccc	9
5	00 04 01.8	+68 34 00.1		22.786 ± 0.074	18.087 ± 0.007	21.7	00040176+6833599	15.423 ± 0.048	13.756 ± 0.035	12.639 ± 0.033	AAA	000	10
6	00 04 01.8	+68 34 34.3	18.906 ± 0.009	16.950 ± 0.005	13.991 ± 0.004	20.9	00040183+6834344	11.359 ± 0.049	10.059 ± 0.051	9.099 ± 0.039	EEE	000	12
7	00 04 02.6	+68 34 26.0		19.489 ± 0.036	16.795 ± 0.011	19.4	00040261+6834263	14.644 ± 0.045	13.355 ± 0.040	12.617 ± 0.033	AAA	ccc	14
8	00 04 07.6	+68 33 24.8	22.113 ± 0.046	19.673 ± 0.006	16.363 ± 0.002	18.2	00040758+6833250	14.158 ± 0.026	12.990 ± 0.032	12.539 ± 0.028	AAA	000	21
9	00 04 11.7	+68 33 25.2		20.455 ± 0.008	16.470 ± 0.003	18.2	00041165+6833253	14.104 ± 0.034	12.978 ± 0.030	12.461 ± 0.021	AAA	000	22
10	00 04 15.2	+68 33 01.8	18.424 ± 0.01	16.617 ± 0.004	14.148 ± 0.002	18.2	00041520+6833019	12.126 ± 0.032	11.019 ± 0.032	10.324 ± 0.023	AAA	000	25
11	00 03 58.4	+68 34 06.6		20.695 ± 0.040	17.521 ± 0.012	6.8	00035828+6834062	14.661 ± 0.034	13.175 ± 0.029	12.276 ± 0.023	AAA	000	7
12	00 04 04.6	+68 34 52.0	21.649 ± 0.033	19.356 ± 0.004	16.025 ± 0.004	23.2	00040454+6834519	13.599 ± 0.029	12.364 ± 0.029	11.625 ± 0.019	AAA	000	16
13	00 04 05.6	+68 33 44.3		17.352 ± 0.013	14.926 ± 0.003	804.5	00040563+6833442	12.867 ± 0.035	11.660 ± 0.032	10.787 ± 0.023	AAA	000	19
14	00 03 38.0	+68 34 55.6		21.268 ± 0.017	17.758 ± 0.006		00033798+6834554	15.120 ± 0.047	14.215 ± 0.048	13.660 ± 0.045	AAA	000	
15	00 03 54.5	+68 33 43.2		23.591 ± 0.127	18.730 ± 0.007		00035445+6833444	14.951 ± 0.047	13.762 ± 0.050	13.027 ± 0.044	AAA	000	
16	00 04 14.0	+68 32 21.5	21.74 ± 0.029	19.904 ± 0.005	17.020 ± 0.003	238.6	00041398+6832215	14.026 ± 0.031	12.709 ± 0.051	11.810 ± 0.033	AAA	000	23
17	00 04 14.7	+68 32 48.8		21.905 ± 0.025	18.924 ± 0.007		00041473+6832490	13.585 ± 0.026	12.480 ± 0.032	12.052 ± 0.021	AAA	000	24
BRC 11NE													
18	02 51 37.4	+60 06 26.6	20.088 ± 0.007	18.481 ± 0.002	16.268 ± 0.002	27.4	02513737+6006267	14.550 ± 0.042	13.527 ± 0.043	12.940 ± 0.033	AAA	000	1
19	02 51 54.5	+60 08 26.6	20.497 ± 0.010	18.837 ± 0.004	16.530 ± 0.003	50.9	02515451+6008266	14.582 ± 0.056	13.567 ± 0.043	12.825 ± 0.038	AAA	c0c	4
20	02 51 58.7	+60 08 05.8	21.109 ± 0.018	19.503 ± 0.004	16.996 ± 0.003	6.8	02515869+6008060	14.918 ± 0.029	14.016 ± 0.043	13.466 ± 0.040	AAA	000	5
21	02 52 11.1	+60 07 15.2	21.649 ± 0.029	19.860 ± 0.005	17.332 ± 0.002	25.5	02521113+6007154	15.634 ± 0.053	14.509 ± 0.058	13.988 ± 0.050	AAA	000	7
22	02 52 15.1	+60 05 18.5	21.220 ± 0.023	19.797 ± 0.008	17.153 ± 0.005	17.9	02521503+6005188	15.113 ± 0.047	14.089 ± 0.042	13.640 ± 0.044	AAA	000	8
23	02 51 54.2	+60 07 43.5	20.456 ± 0.012	18.598 ± 0.006	15.919 ± 0.003		02515419+6007437	14.116 ± 0.034	13.144 ± 0.037	12.791 ± 0.033	AAA	000	3
24	02 51 59.7	+60 06 39.3	20.803 ± 0.012	19.202 ± 0.004	16.893 ± 0.002	49.4	02515975+6006394	15.306 ± 0.048	14.236 ± 0.042	13.515 ± 0.038	AAA	000	6
25	02 51 52.1	+60 07 10.0	19.964 ± 0.009	18.334 ± 0.003	15.988 ± 0.002		02515212+6007102	14.131 ± 0.032	12.975 ± 0.033	12.136 ± 0.026	AAA	000	
26	02 52 01.3	+60 06 15.3		21.882 ± 0.028	18.491 ± 0.004		02520131+6006154	15.629 ± 0.053	14.406 ± 0.056	13.627 ± 0.042	AAA	000	
27	02 51 59.9	+60 05 32.0		21.713 ± 0.021	18.551 ± 0.006		02515993+6005323	16.155 ± 0.091	14.914 ± 0.081	14.142 ± 0.068	AAA	000	
BRC 11													
28	02 51 32.8	+60 03 54.3		19.871 ± 0.013	16.965 ± 0.012	7.2	02513283+6003542	13.005 ± 0.026	11.523 ± 0.032	10.447 ± 0.022	AAA	000	1
29	02 51 25.6	+60 06 04.8	19.816 ± 0.006	18.318 ± 0.002	15.967 ± 0.001		02512557+6006048	14.609 ± 0.038	13.142 ± 0.033	12.095 ± 0.019	AAA	000	
BRC 11E													
30	02 52 13.6	+60 03 26.2		20.991 ± 0.014	18.151 ± 0.015	136.4	02521362+6003262	15.592 ± 0.074	14.685 ± 0.064	14.157 ± 0.072	AAA	ccc	1
31	02 52 14.2	+60 03 11.7	20.687 ± 0.016	19.129 ± 0.005	16.647 ± 0.008		02521422+6003114	14.311 ± 0.036	13.278 ± 0.038	12.532 ± 0.032	AAA	000	
	BRC 13												
32	03 00 51.1	+60 39 36.3	20.129 ± 0.014	18.477 ± 0.022		99.2	03005107+6039360	13.508 ± 0.044	12.421 ± 0.043	11.804 ± 0.038	AAA	ccc	6
33	03 00 51.6	+60 39 48.9		21.683 ± 0.031	17.783 ± 0.003	20.5	03005161+6039489	15.270 ± 0.055	14.176 ± 0.044	13.478 ± 0.068	AAA	c00	7
34	03 00 52.7	+60 39 31.6	21.216 ± 0.018	19.667 ± 0.006	17.147 ± 0.003	602.3	03005265+6039317	15.043 ± 0.050	14.025 ± 0.050	13.291 ± 0.042	AAA	000	10
35	03 00 53.6	+60 40 24.9	21.955 ± 0.042	19.702 ± 0.013	16.893 ± 0.009		03005350+6040252	14.376 ± 0.042	13.157 ± 0.045	12.751 ± 0.038	AAA	ccc	11
36	03 00 55.4	+60 39 42.7		20.841 ± 0.015	17.869 ± 0.004	180.5	03005542+6039427	15.789 ± 0.075	14.496 ± 0.059	13.935 ± 0.056	AAA	000	12

Table 3 – *continued*

S. no.	RA (2000)	Dec. (2000)	$B \pm eB$ (mag)	$V \pm eV$ (mag)	$I_c \pm eI_c$ (mag)	EW [Hα] (Å)	2MASS name	J ± eJ (mag)	$H \pm eH$ (mag)	K ± eK (mag)	Q flag	C flag	ID(Ogura et al. 2002)
37	03 00 56.0	+60 40 26.3		20.713 ± 0.022	17.244 ± 0.008	8.0	03005601+6040265	14.695 ± 0.053	13.591 ± 0.057	12.945 ± 0.054	AAA	cc0	13
38	03 00 44.8	+60 40 09.1	21.874 ± 0.038	19.923 ± 0.009	17.283 ± 0.015	16.7	03004476+6040092	14.683 ± 0.039	13.756 ± 0.039	13.008 ± 0.036	AAA	000	2
39	03 00 45.3	+60 40 39.5	20.536 ± 0.01	18.722 ± 0.005	16.399 ± 0.004	14.8	03004529+6040395	14.517 ± 0.038	13.672 ± 0.038	13.327 ± 0.040	AAA	000	3
BRC 14													
40	03 01 24.0	+60 30 42.2		21.397 ± 0.029	17.971 ± 0.005	125.4	03012400+6030423	15.940 ± 0.010	14.870 ± 0.010	14.410 ± 0.010			29
41	03 01 24.7	+60 30 09.6		21.998 ± 0.045	18.197 ± 0.006			15.680 ± 0.010	14.360 ± 0.010	13.780 ± 0.010			30
42	03 01 25.6	+60 29 39.0		19.644 ± 0.006	16.857 ± 0.003	9.5	03012556+6029392	14.730 ± 0.010	13.610 ± 0.010	13.080 ± 0.010			31
43	03 01 26.4	+60 30 53.9	20.374± 0.012	18.351 ± 0.003	15.816 ± 0.004	10.6	03012638+6030539	14.050 ± 0.010	13.030 ± 0.010	12.570 ± 0.010			32
44	03 01 27.2	+60 30 56.9		20.927 ± 0.018	18.063 ± 0.006	58.5	03012722+6030569	16.150 ± 0.020	15.090 ± 0.020	14.520 ± 0.020			33
45	03 01 27.4	+60 30 39.7	22.791± 0.092	20.661 ± 0.016	17.794 ± 0.006	21.3		15.510 ± 0.010	14.370 ± 0.010	13.820 ± 0.010			34
46	03 01 29.3	+60 31 13.6	20.097± 0.009	18.277 ± 0.003	15.866 ± 0.002	49.4	03012930+6031136	14.720 ± 0.010	13.420 ± 0.010	12.420 ± 0.010			35
47	03 01 34.0	+60 27 45.6	22.614± 0.076	20.349 ± 0.011	17.343 ± 0.003	11.4		15.200 ± 0.010	14.190 ± 0.010	13.700 ± 0.010			39
48	03 01 34.4	+60 30 08.5		20.462 ± 0.012	17.100 ± 0.003	19.4		14.750 ± 0.010	13.410 ± 0.010	12.680 ± 0.010			40
49	03 01 36.4	+60 29 06.1		21.481 ± 0.034	17.928 ± 0.005	54.7	03013640+6029061	15.660 ± 0.010	14.180 ± 0.010	13.120 ± 0.010			41
50	03 01 37.0	+60 31 00.2		20.347 ± 0.012	17.175 ± 0.017	17.1	03013695+603100	14.920 ± 0.010	13.880 ± 0.010	13.360 ± 0.010			42
51	03 01 37.1	+60 29 41.2		20.355 ± 0.010	17.228 ± 0.004	6.5		15.770 ± 0.010	15.160 ± 0.020	14.870 ± 0.020			43
52	03 01 43.3	+60 28 51.5		22.110 ± 0.051	18.337 ± 0.012	13.3		15.530 ± 0.010	14.030 ± 0.010	13.240 ± 0.010			46
53	03 01 50.0	+60 28 50.5		21.694 ± 0.032	18.183 ±0.006			15.650± 0.010	14.310± 0.010	13.800± 0.010			47
54	03 01 04.2	+60 31 25.3		20.579 ± 0.016	17.760 ± 0.004	44.8	03010418+6031252	15.640 ± 0.010	14.460 ± 0.010	13.800 ± 0.010			1
55	03 01 06.2	+60 30 17.6	22.387 ± 0.062	20.709 ± 0.017	17.481 ± 0.008	79.8	03010623+6030176	15.670 ± 0.010	14.610 ± 0.010	14.070 ± 0.010			3
56	03 01 06.6	+60 30 36.0		22.287 ± 0.067	18.596 ± 0.006			16.420 ± 0.020	15.420 ± 0.020	14.900 ± 0.020			4
57	03 01 07.7	+60 29 21.8	20.223 ± 0.011	18.335 ± 0.002	15.968 ± 0.003	31.5	03010774+6029218	14.300 ± 0.010	13.150 ± 0.010	12.340 ± 0.010			5
58	03 01 11.5	+60 30 46.3		20.875 ± 0.024	17.987 ± 0.018	86.6	03011150+6030464	16.100 ± 0.020	15.070 ± 0.020	14.490 ± 0.010			6
59	03 01 13.4	+60 29 31.9		21.807 ± 0.040	18.383 ± 0.006	13.7		15.550 ± 0.010	14.350 ± 0.010	13.690 ± 0.010			8
60	03 01 16.1	+60 29 47.1		21.138 ± 0.023	17.779 ± 0.004	25.8	03011610+6029470	15.820 ± 0.010	14.770 ± 0.010	14.280 ± 0.010			10
61	03 01 17.0	+60 29 23.2	22.261 ± 0.058	19.904 ± 0.008	17.179 ± 0.003	16.0	03011705+6029232	15.350 ± 0.010	14.360 ± 0.010	13.970 ± 0.010			12
62	03 01 20.3	+60 30 02.3		20.338 ± 0.012	17.666 ± 0.003	38.4	03012024+6030024	15.580 ± 0.010	14.310 ± 0.010	13.330 ± 0.010			18
63	03 01 20.6	+60 29 31.7	22.594 ± 0.079	20.767 ± 0.019	17.990 ± 0.004	9.1		15.750 ± 0.010	14.690 ± 0.010	14.150 ± 0.010			20
64	03 01 21.2	+60 29 44.3		20.297 ± 0.017	17.608 ± 0.005			15.790 ± 0.010	14.670 ± 0.010	14.040 ± 0.010			23
65	03 01 21.2	+60 30 10.5		20.969 ± 0.018	17.774 ± 0.004	24.3		15.880 ± 0.010	14.750 ± 0.010	13.970 ± 0.010			24
66	03 01 32.0	+60 29 36.3		21.907 ± 0.046	19.193 ± 0.015			17.600 ± 0.020	16.550 ± 0.030	15.720 ± 0.030			
67	03 01 21.9	+60 29 29.5		20.588 ± 0.013	17.660 ± 0.004		03012186+6029296	15.630 ± 0.070	14.700 ± 0.070	14.150 ± 0.070	AAA	000	
68	03 01 51.4	+60 27 22.7		22.305 ± 0.059	18.613 ± 0.008		03015137+6027224	15.590 ± 0.073	14.560 ± 0.070	13.900 ± 0.050	AAA	000	
69	03 01 19.4	+60 29 38.9		21.924 ± 0.042	19.621 ± 0.016			17.730 ± 0.020	16.71 ± 0.010	15.930 ± 0.010			
70	03 00 47.1	+60 28 53.6		20.298 ± 0.011	17.664 ± 0.019		03004713+6028535	15.030 ± 0.050	14.05 ± 0.060	13.386 ± 0.053	AAA	ccc	
71	03 01 20.3	+60 29 49.3	15.932 ±0.008	14.746 ± 0.015	13.256 ± 0.026		03012029+6029493	11.910 ± 0.028	10.97 ± 0.030	10.171 ± 0.023	AAA	000	
72	03 01 23.5	+60 31 50.6		20.853 ± 0.021	18.096 ± 0.005		03012352+6031507	16.070 ± 0.100	15.02 ± 0.090	14.330 ± 0.072	AAA	000	
73	03 01 14.1	+60 29 37.4		21.553 ± 0.034	19.196 ± 0.017			17.370 ± 0.010	16.39 ± 0.010	15.590 ± 0.010			
74	03 01 01.1	+60 30 45.2		21.045 ± 0.024	19.013 ± 0.020			16.770 ± 0.010	15.64 ± 0.010	14.840 ± 0.010			
75	03 00 58.0	+60 30 13.4		19.776 ± 0.012	17.100 ± 0.021		03005792+6030133	14.930 ± 0.046	13.89 ± 0.050	13.158 ± 0.039	AAA	000	
76	03 01 00.9	+60 33 26.7		20.708 ± 0.021	17.603 ± 0.005		03010092+6033265	15.680 ± 0.076	14.85 ± 0.090	14.324 ± 0.098	AAA	000	
77	03 01 02.9	+60 31 22.4		21.023 ± 0.025	18.045 ± 0.005		03010291+6031223	15.880 ± 0.093	15.02 ± 0.104	14.438 ± 0.097	AAA	000	
78	03 00 57.9	+60 31 21.7		20.848 ± 0.021	17.721 ± 0.004		03005798+6031217	15.970 ± 0.090	15.10 ± 0.092	14.550 ± 0.099	AAA	000	

Table 3 – *continued*

S. no.	RA (2000)	Dec. (2000)	$B \pm eB$ (mag)	$V \pm eV$ (mag)	$I_c \pm eI_c$ (mag)	EW [Hα] (Å)	2MASS name	J ± eJ (mag)	$H \pm eH$ (mag)	K ± eK (mag)	Q flag	C flag	ID(Ogura et al. 2002)
79	03 00 51.8	+60 32 10.8		20.733 ± 0.019	17.931 ± 0.004		03005180+6032106	15.830 ± 0.097	14.89 ± 0.101	14.270 ± 0.089	AAA	ccc	
80	03 01 05.2	+60 31 55.4	17.823 ± 0.002	16.269 ± 0.001	14.261 ± 0.005		03010520+6031552	12.780 ± 0.020	11.88 ± 0.030	11.312 ± 0.022	AAA	000	
BRC 27													
81	07 03 52.8	−11 23 13.2	18.954±0.018	17.465 ± 0.015	15.313 ± 0.028	4.6	07035271-1123132	13.801 ± 0.047	13.026 ± 0.050	12.848 ± 0.039	AAA	000	2
82	07 03 53.8	−11 24 28.4		20.018 ± 0.009	16.761 ± 0.002	27.7	07035372-1124285	15.008 ± 0.043	14.211 ± 0.051	13.960 ± 0.057	AAA	000	4
83	07 03 57.1	−11 24 32.8	20.764±0.069	19.139 ± 0.005	16.476 ± 0.004	6.1	07035712-1124327	14.789 ± 0.033	13.968 ± 0.021	13.756 ± 0.053	AAA	000	7
84	07 04 02.9	−11 23 37.3	20.678±0.085	19.011 ± 0.014	16.327 ± 0.015	8.4	07040290-1123375	13.489 ± 0.043	12.400 ± 0.049	11.875 ± 0.033	AAA	000	8
85	07 04 03.1	−11 23 50.6		20.176 ± 0.011	17.398 ± 0.003	72.6	07040308-1123504	15.583 ± 0.060	14.303 ± 0.043	13.567 ± 0.040	AAA	000	10
86	07 04 04.3	−11 23 55.7	20.895±0.074	19.616 ± 0.011	16.722 ± 0.004	168.3	07040426-1123556	14.949 ± 0.044	13.995 ± 0.042	13.559 ± 0.047	AAA	000	12
87	07 04 04.8	−11 23 39.8	20.026±0.036	18.318 ± 0.003	15.970 ± 0.003	26.6	07040470-1123397	14.089 ± 0.040	13.060 ± 0.043	12.527 ± 0.037	AAA	000	14
88	07 04 05.3	−11 23 13.2	20.508±0.049	19.095 ± 0.004	16.546 ± 0.003	38.8	07040519-1123132	14.393 ± 0.071	13.226 ± 0.073	12.472 ± 0.040	AAA	000	15
89	07 04 06.0	−11 23 58.9	19.815±0.030	18.224 ± 0.006	15.925 ± 0.004	22.0	07040593-1123587	14.360 ± 0.033	13.444 ± 0.026	12.951 ± 0.031	AAA	000	16
90	07 04 06.0	−11 23 15.7		20.053 ± 0.008	17.314 ± 0.003	4.2	07040603-1123156	15.030 ± 0.062	13.933 ± 0.044	13.264 ± 0.035	AAA	000	17
91	07 04 06.5	−11 23 36.2		20.585 ± 0.013	16.839 ± 0.003	318.1	07040644-1123360	14.652 ± 0.049	13.788 ± 0.050	13.381 ± 0.072	AAA	ccc	18
92	07 04 06.5	−11 23 16.4	19.70±0.026	18.083 ± 0.003	15.744 ± 0.002	33.8	07040656-1123163	13.851 ± 0.062	12.932 ± 0.043	12.543 ± 0.031	AAA	c00	19
93	07 03 52.6	−11 26 16.8	18.311 ± 0.010	16.865 ± 0.002	15.109 ± 0.002	19.8	07035249-1126168	13.657 ± 0.027	12.855 ± 0.030	12.588± 0.029	AAA	000	1
94	07 03 55.0	−11 25 14.5	20.349 ± 0.045	18.769 ± 0.004	16.153 ± 0.009	4.6	07035499-1125145	14.593 ± 0.030	13.817 ± 0.040	13.600± 0.047	AAA	000	5
95	07 03 56.4	−11 25 41.5		20.435 ± 0.019	17.396 ± 0.008	11.0	07035638-1125413	15.671 ± 0.073	14.931 ± 0.070	14.439± 0.088	AAA	000	6
96	07 04 04.1	−11 26 35.5		20.515 ± 0.091	17.267 ± 0.021	36.1	07040408-1126354	15.349 ± 0.048	14.595 ± 0.070	14.146± 0.062	AAA	000	11
97	07 04 08.2	−11 23 54.6	17.168± 0.006	15.949 ± 0.003	14.346 ± 0.002	39.1	07040803-1123547	13.094 ± 0.033	12.430 ± 0.037	12.216± 0.030	AAA	000	22
98	07 04 08.2	−11 23 09.6	21.783± 0.144	20.338 ± 0.008	17.413 ± 0.003	926.8	07040816-1123097	15.411 ± 0.111	14.568 ± 0.055	14.205± 0.075	EAA	ccc	23
99	07 04 09.4	−11 24 38.1		21.053 ± 0.013	17.261 ± 0.003	137.2	07040925-1124381	15.003 ± 0.039	14.222 ± 0.054	13.729± 0.053	AAA	ccc	24
100	07 04 09.8	−11 23 16.4	16.234± 0.004	15.106 ± 0.002	13.525 ± 0.003	53.2	07040995-1123164	11.698 ± 0.024	10.663 ± 0.021	9.849 ± 0.021	AAA	ccc	25
101	07 04 12.0	−11 24 23.0		20.330 ± 0.014	16.850 ± 0.004	69.5	07041195-1124227	14.658 ± 0.047	13.866 ± 0.054	13.473± 0.047	AAA	ccc	27
102	07 04 13.0	−11 24 03.2	19.017± 0.016	17.570 ± 0.002	15.695 ± 0.003	293.7	07041292-1124031	15.317 ± 0.060	14.369 ± 0.047	13.931± 0.047	AAA	000	28
103	07 04 13.4	−11 24 55.8	16.822± 0.005	15.519 ± 0.003	13.742 ± 0.004	17.5	07041352-1124557	12.135 ± 0.028	11.269 ± 0.024	10.795± 0.023	AAA	000	29
104	07 04 14.2	−11 23 17.2	18.986± 0.016	17.596 ± 0.002	15.548 ± 0.002	33.1	07041424-1123169	13.833 ± 0.028	12.949 ± 0.022	12.358± 0.026	AAA	000	31
105	07 04 14.2	−11 23 37.3		20.843 ± 0.025	17.507 ± 0.004		07041427-1123371	15.435 ± 0.064	14.551 ± 0.060	14.034 ± 0.059	AAA	000	32
106	07 04 08.4	−11 20 05.3	13.529± 0.028	12.533 ± 0.026	11.936 ± 0.024		07040831-1120052	13.600 ± 0.028	12.564 ± 0.026	11.919 ± 0.024	AAA	000	
107	07 04 03.1	−11 23 27.6	12.919± 0.038	11.533 ± 0.037	10.710 ± 0.026		07040314-1123275	13.033 ± 0.038	11.573 ± 0.037	10.694 ± 0.026	AAA	000	
108	07 03 54.7	−11 20 11.0	15.869± 0.074	14.946± 0.076	14.385 ± 0.074		07035465-1120110	15.933 ± 0.074	14.976 ± 0.076	14.368 ± 0.074	AAA	000	
109	07 03 52.3	−11 21 01.1	15.618± 0.065	14.546 ± 0.068	13.794 ± 0.050		07035228-1121009	15.705 ± 0.065	14.586 ± 0.068	13.777 ± 0.050	AAA	000	
110	07 04 12.2	−11 20 20.8	15.618± 0.065	14.546 ± 0.068	13.794 ± 0.050		07041215-1120205	15.848 ± 0.072	14.463 ± 0.049	13.640 ± 0.040	AAA	000	
111	07 04 05.8	−11 20 03.8	15.743± 0.072	14.426 ± 0.049	13.656 ± 0.040		07040576-1120038	14.827 ± 0.048	13.459 ± 0.037	12.631 ± 0.030	AAA	000	
112	07 04 16.8	−11 24 32.4	14.723± 0.048	13.421 ± 0.037	12.647 ± 0.030		07041680-1124324	14.123 ± 0.026	13.213 ± 0.028	12.595 ± 0.024	AAA	000	
113	07 04 15.1	−11 26 22.6	14.062± 0.026	13.182 ± 0.028	12.612 ± 0.024		07041508-1126224	14.151 ± 0.033	13.094 ± 0.032	12.441 ± 0.027	AAA	000	
114	07 04 19.9	−11 22 22.4	14.078± 0.033	13.063 ± 0.032	12.458 ± 0.027		07041999-1122224	14.352 ± 0.029	13.340 ± 0.024	12.666 ± 0.029	AAA	000	
115	07 04 15.1	−11 23 39.8	16.111± 0.086	15.008 ± 0.076	14.249 ± 0.075		07041500-1123398	16.200 ± 0.086	15.049 ± 0.076	14.232 ± 0.075	AAA	c00	
BRC 38													
116	21 40 26.2	+58 14 24.7	22.249 ± 0.032	20.232 ± 0.014	17.812 ± 0.012		21402612+5814243	15.182 ± 0.076	14.262 ± 0.051	14.004 ± 0.062	AAA	000	1
117	21 40 28.1	+58 15 14.4	0 ± 0	20.2 ± 0.011	17.296 ± 0.013	23.94	21402800+5815142	14.506 ± 0.038	13.411 ± 0.035	12.939 ± 0.035	AAA	000	3
118	21 40 31.7	+58 17 55.3	22.632 ± 0.047	20.275 ± 0.012	17.054 ± 0.008	3.04	21403159+5817551	14.028 ± 0.032	12.889 ± 0.031	12.393 ± 0.028	AAA	000	4
119	21 40 37.0	+58 14 38.0	18.448 ± 0.012	16.664 ± 0.004	14.441 ± 0.015	55.86	21403691+5814378	11.902 ± 0.024	10.886 ± 0.030	10.234 ± 0.018	AAA	000	6
120	21 40 37.0	+58 15 03.2	21.957 ± 0.027	20.142 ± 0.011	17.069 ± 0.01	25.84	21403704+5815029	14.269 ± 0.029	13.284 ± 0.041	12.821 ± 0.029	AAA	000	7

Table 3 – *continued*

S. no.	RA (2000)	Dec. (2000)	$B \pm eB$ (mag)	$V \pm eV$ (mag)	$I_c \pm eI_c$ (mag)	EW [Hα] (Å)	2MASS name	J ± eJ (mag)	$H \pm eH$ (mag)	K ± eK (mag)	Q flag	C flag	ID(Ogura et al. 2002)
121	21 40 41.3	+58 15 11.5	19.971 ± 0.011	18.055 ± 0.005	15.403 ± 0.011	25.08	21404116+5815112	12.968 ± 0.031	11.614 ± 0.035	10.676 ± 0.019	AAA	000	9
122	21 40 41.5	+58 14 25.8	22.43 ± 0.046	20.582 ± 0.016	17.642 ± 0.015	14.06	21404156+5814255	13.650 ± 0.029	12.618 ± 0.032	12.166 ± 0.028	AAA	000	10
123	21 40 44.9	+58 15 03.6	0	21.232 ± 0.023	17.95 ± 0.015	113.24	21404485+5815033	14.617 ± 0.038	13.347 ± 0.040	12.658 ± 0.030	AAA	000	11
124	21 40 48.0	+58 15 37.8	22.524 ± 0.037	20.546 ± 0.015	16.845 ± 0.01	16.34	21404803+5815376	13.894 ± 0.026	12.954 ± 0.033	12.667 ± 0.028	AAA	000	12
125	21 40 49.0	+58 17 09.6	0	21.541 ± 0.033	17.932 ± 0.012	59.66	21404908+5817093	14.141 ± 0.031	12.859 ± 0.038	12.133 ± 0.018	AAA	000	15
126	21 40 27.4	+58 14 21.5	21.205 ± 0.02	19.702 ± 0.013	17.041 ± 0.017	57.00	21402732+5814212	14.303 ± 0.042	13.303 ± 0.040	12.878 ± 0.039	AAA	000	2
127	21 40 36.5	+58 13 46.2	21.377 ± 0.016	19.213 ± 0.007	16.289 ± 0.024	4.18	21403655+5813458	13.514 ± 0.024	12.582 ± 0.032	12.245 ± 0.026	AAA	000	5
128	21 40 42.7	+58 19 37.6	0.	21.135 ± 0.021	17.456 ± 0.014		21404282+5819373	13.935 ± 0.032	12.545 ± 0.036	11.640 ± 0.024	AAA	000	
129	21 41 12.0	+58 20 33.7	0.	21.726 ± 0.037	18.972 ± 0.021		21411208+5820336	16.171 ± 0.098	15.152 ± 0.089	14.523 ± 0.090	AAA	000	
130	21 40 45.1	+58 19 50.2	0.	22.364 ± 0.093	18.643 ± 0.011		21404517+5819506	14.668 ± 0.026	13.121 ± 0.030	12.214 ± 0.019	AAA	000	
131	21 39 49.2	+58 14 37.0	23.277 ± 0.176	21.125 ± 0.029	17.511 ± 0.024		21394918+5814365	14.592 ± 0.026	13.607 ± 0.037	12.934 ± 0.023	AAA	000	
132	21 39 56.4	+58 13 47.7	20.981 ± 0.021	19.037 ± 0.014	16.289 ± 0.024		21395635+5813475	13.338 ± 0.028	12.273 ± 0.036	11.528 ± 0.023	AAA	000	
133	21 40 21.8	+58 14 45.6	23.012 ± 0.068	21.092 ± 0.023	17.536 ± 0.007		21402176+5814454	14.784 ± 0.036	13.775 ± 0.047	13.043 ± 0.028	AAA	000	

designated as BRC 11NE and BRC 11E, respectively, by Ogura et al. (2002). They are not listed in SFO91 because of the lack of associated IRAS point sources. However, Ogura et al. (2002) found several Hα emission stars in the vicinity of BRC 11NE in contrast to one or two in and around BRC 11 and BRC 11E. Moreover, BRC 11NE appears to be associated with a more or less clear aggregate of young stars just outside its tip. So BRC 11NE was selected as one of the target BRCs in Paper I to show an age gradient. In the present study, we have aimed to increase the sample stars for age determination by reaching a deeper limiting magnitude.

BRC 14 is associated with the molecular cloud IC 1848A to its east, which harbours a bright IR young cluster AFGL 4029 (Deharveng et al. 1997). The optical and NIR study by these authors revealed that AFGL 4029 is an active star formation site. A deeper NIR survey of the BRC 14 region by Matsuyanagi et al. (2006) supports sequential star formation in this region propagating from the west. Paper I determined the ages of the stars associated with BRC 14 and found a quantitative evidence for the S^4F hypothesis. We are repeating the study with deeper data for this BRC too.

BRC 27. BRC 27 is located at the outer edge of S296 at a distance of 1.15 kpc (SFO91) and associated with the active star-forming region Canis Major R1 (CMa R1). The location of S296 coincides with the boundary of an expanding neutral hydrogen shell. Shevchenko et al. (1999) have estimated the ages of the stellar contents of CMa R1 ranging from <1 Myr to 8 Myr. Herbst & Assousa (1977) suggested that the star formation in the CMa R1 region could have been triggered by a supernova explosion.

BRC 38. Cepheus OB2, located at a distance of ~870 pc (Contreras et al. 2002), is a complex of a stellar aggregate and a bubble-shaped structure of atomic and molecular gas (Patel et al. 1994, 1998). The clusters NGC 7160 and Tr 37 are located near the centre of the bubble and near its edge, respectively. There is evidence that the star formation at the edge of the bubble was triggered by a supernova explosion which took place near the centre of the bubble (Sicilia-Aguilar et al. 2004, 2005). Tr 37 harbours an O6 star HD 206267, which excites the relatively evolved H II region IC 1396. The age of Tr 37 is estimated as ~3–5 Myr (Contreras et al. 2002). IC 1396 has a rich population of BRCs including BRCs 32-42 (SFO91), among which BRCs 37 and 38 have been studied extensively (see e.g. Getman et al. 2007; Ikeda et al. 2008). In particular, Paper I reported quantitative evidence for S^4F in BRC 37, and Ikeda et al. (2008) confirmed sequential star formation in this region. Getman et al. (2007) provided detailed qualitative discussion on S^4F based on the *Chandra* X-ray data for BRC 38.

5 MEMBERSHIP AND AGE DETERMINATION OF MEMBER STARS

The aggregates associated with BRCs are very loose and are composed of a small number of stars. Since BRCs are found at low galactic latitudes, the fields can be significantly contaminated by foreground/background stars. To understand star formation in BRCs, it is necessary to identify stars directly related to them. We selected probable members associated with the BRCs using the following criteria.

The spectra of some pre-main-sequence (PMS) stars, specifically classical T-Tauri stars (CTTSs), show emission lines, among which usually Hα is the strongest. Therefore, Hα emission stars can be considered as good candidates for PMS stars associated with BRCs. In the present study we use Hα emission stars found by Ogura et al. (2002) in the vicinity of BRCs. However, some of them may not be directly associated with the BRCs (see Section 6.3).

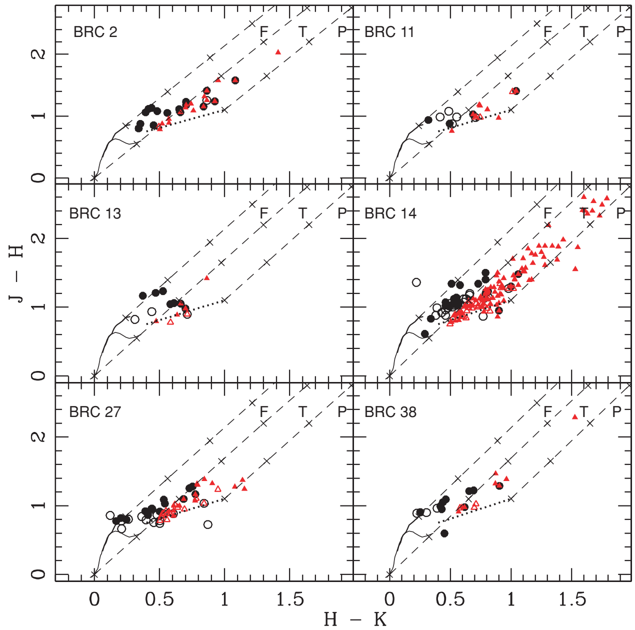

Figure 1. $(J-H)/(H-K)$ colour–colour diagrams for BRCs 2, 11NE, 13, 14, 27 and 38. The sequences for dwarfs (thin solid curve) and giants (thick solid curve) are from Bessell & Brett (1988). The dotted line represents the intrinsic locus of CTTSs (Meyer et al. 1997). The three parallel dashed lines represent the reddening vectors. The crosses on the dashed lines are separated by $A_V = 5$ mag. The open and filled circles are Hα emission stars lying in outside and on/inside the bright rims (see Fig. A1), respectively. The open and filled triangles are NIR excess stars lying in outside and on/inside the bright rims, respectively.

Since many PMS stars also show NIR excesses caused by circumstellar discs, NIR photometric surveys have also emerged as a powerful tool to detect low-mass PMS stars. To identify NIR excess stars from the 2MASS PSC, we used NIR $(J-H)/(H-K)$ colour–colour (NIR-CC) diagrams. Fig. 1 shows NIR-CC diagrams for the studied BRCs. The thin and thick solid curves represent the unreddened main-sequence and giant branches (Bessell & Brett 1988), respectively. The dotted line indicates the locus of intrinsic CTTSs (Meyer, Calvet & Hillenbrand 1997). The curves are also in the CIT system. The parallel dashed lines are the reddening vectors drawn from the tip (spectral type M4) of the giant branch ('upper reddening line'), from the base (spectral type A0) of the main-sequence branch ('middle reddening line') and from the tip of the intrinsic CTTS line ('lower reddening line'). The extinction ratios $A_J/A_V = 0.265$, $A_H/A_V = 0.155$ and $A_K/A_V = 0.090$ have been adopted from Cohen et al. (1981). We classified sources into three regions in the NIR-CC diagrams (cf. Ojha et al. 2004a). 'F' sources are located between the upper and middle reddening lines and are considered to be either field stars (main-sequence stars, giants) or Class III and Class II sources with small NIR excesses. 'T' sources are located between the middle and lower reddening lines. These sources are considered to be mostly CTTSs (Class II objects). There may be an overlap in NIR colours of Herbig Ae/Be stars and CTTSs in the 'T' region (Hillenbrand et al. 1992). 'P' sources are those located in the region redward of the 'T' region and are most likely Class I objects (protostar-like objects; Ojha et al. 2004b). So, objects falling in the 'T' and 'P' regions of NIR-CC diagrams are considered as NIR excess stars and probable members of the BRC aggregates. These are included in the analysis of the present study in addition to Hα emission stars. However, we selected only those Hα emission stars, as probable members associated with the BRCs, that lie rightward of the upper reddening line. It is worthwhile, however, to mention that Robitaille et al. (2006) have recently shown that there is a significant overlap between protostars and CTTSs in the NIR-CC space.

The spatial distribution of the probable YSOs (i.e. Hα emission and NIR excess stars) for each BRC is shown in Fig. A1, which is available in electronic form only. In Fig. A1, we have also demarcated the two regions for each BRC, i.e. on/inside and outside the bright rim. The NIR-CC diagrams (Fig. 1) were used to estimate A_V for each of these stars by tracing back to the intrinsic CTTS line of Meyer et al. (1997) along the reddening vector (for details see, Paper I). The A_V for stars lying in the 'F' region is estimated by tracing them back to the extension of the intrinsic CTTS line. Fig. 2 shows dereddened V_0, $(V-I_c)_0$ colour–magnitude (CM) diagrams for those stars.

In Fig. 2, the post-main-sequence isochrone for 2 Myr by Girardi et al. (2002), which is practically a ZAMS line, and PMS isochrones for 1, 3, 10, 30 Myr for the solar metallicity by Siess, Dufour & Forestini (2000) are also plotted. The distances are taken from SFO 91 barring for BRC 38. In the case of BRC 38 a distance of 870 pc has been adopted from Contreras et al. (2002). The age of each YSO was estimated by referring to the isochrones. The mass of the YSOs was estimated using the $V_0/(V-I_c)_0$ CM diagram as discussed in Pandey et al. (2008). The resultant A_V values, ages and masses are given in Table 4.

The ages range from 0.1 to a few Myr (with some exceptions) which are comparable with the lifetime of TTSs. The masses of these YSOs, range from $\sim$0.1 to 2.0 $M_\odot$, further indicate that they are probable TTSs and their siblings.

Here we would like to point out that the estimation of the ages of the PMS stars by comparing the observations with the

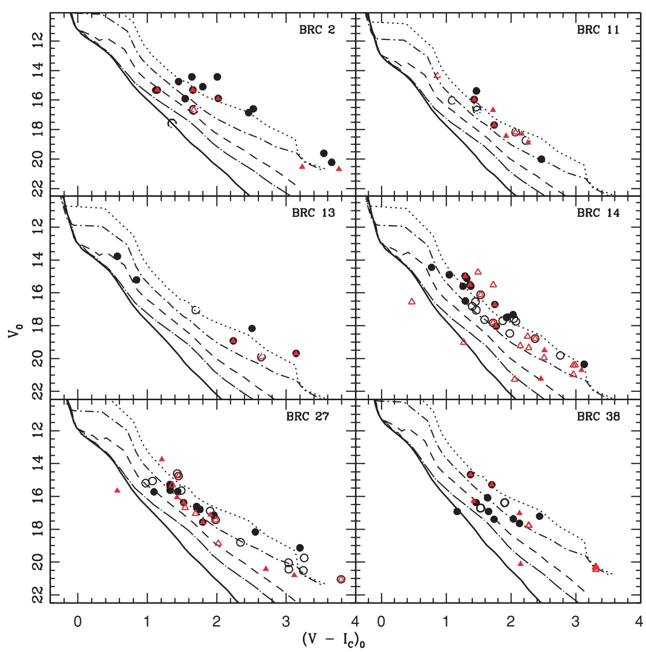

Figure 2. $V_0/(V-I_c)_0$ CM diagrams for probable YSOs in BRCs 2, 11NE,13, 14, 27 and 38. The 2 Myr isochrone (thick curve) by Girardi et al. (2002) and PMS isochrones of 1 (dotted), 3 (dash–dotted), 10 (dashed), 30 (large dash–dotted) Myr by Siess et al. (2000) are also shown. All the isochrones are corrected for the distances of the respective BRCs. The symbols are same as in Fig. 1.

Table 4. Dereddened magnitude, colours, age and mass of the YSOs associated with the BRCs.

S. no.	RA (2000)	Dec. (2000)	V_0 (mag)	$(B-V)_0$ (mag)	$(V-I)_0$ (mag)	$A_V \pm \sigma$ (mag)	Age $\pm\ \sigma$ (Myr)	Mass $\pm\ \sigma$ ($M_\odot$)	ID (Ogura et al. 2002)
BRC 2									
1	00 03 57.1	+68 33 46.4	15.101	1.149	1.800	3.0 ± 0.4	0.7 ± 0.0	0.52 ± 0.01	5
2	00 03 57.3	+68 33 23.0	19.604	–	3.543	2.9 ± 0.5	0.3 ± 0.0	0.14 ± 0.01	6
3	00 03 59.1	+68 32 47.4	20.219	–	3.656	0.9 ± 0.5	0.3 ± 0.0	0.11 ± 0.01	8
4	00 04 01.6	+68 34 14.2	15.911	–	1.546	2.1 ± 0.5	4.0 ± 0.9	0.78 ± 0.06	9
5	00 04 01.8	+68 34 00.1	16.857	–	2.460	5.9 ± 0.5	1.1 ± 0.1	0.30 ± 0.02	10
6	00 04 01.8	+68 34 34.3	14.431	1.246	2.008	2.5 ± 0.6	0.1 ± 0.0	0.47 ± 0.01	12
7	00 04 02.6	+68 34 26.0	15.329	–	1.123	4.2 ± 0.6	16.1 ± 3.0	1.11 ± 0.04	14
8	00 04 07.6	+68 33 24.8	14.750	0.995	1.451	4.9 ± 0.4	1.2 ± 0.1	0.85 ± 0.03	21
9	00 04 11.7	+68 33 25.2	16.596	–	2.527	3.9 ± 0.4	0.2 ± 0.1	0.29 ± 0.00	22
10	00 04 15.2	+68 33 01.8	14.428	1.170	1.643	2.2 ± 0.4	0.6 ± 0.0	0.63 ± 0.01	25
11	00 03 58.4	+68 34 06.6	15.320	–	1.144	5.4 ± 0.4	12.3		7
12	00 04 04.6	+68 34 52.0	15.891	1.298	2.022	3.5 ± 0.4	0.9 ± 0.0	0.40 ± 0.01	16
13	00 04 05.6	+68 33 44.3	15.319	–	1.658	2.0 ± 0.4	1.2 ± 0.1	0.63 ± 0.02	19
14	00 03 38.0	+68 34 55.6	20.526	–	3.231	0.7 ± 0.6	4.5 ± 0.2	0.14 ± 0.02	
15	00 03 54.5	+68 33 43.2	20.680	–	3.761	2.2 ± 0.4	1.0	0.09 ± 0.01	
16	00 04 14.0	+68 32 21.5	16.680	0.921	1.665	3.2 ± 0.5	6.7 ± 1.1	0.68 ± 0.03	23
17	00 04 14.7	+68 32 48.8	17.600	–	1.355	4.3 ± 0.4	>30		24
BRC 11NE									
18	02 51 37.4	+60 06 26.6	16.495	1.028	1.463	2.0 ± 0.6	1.5 ± 0.2	0.91 ± 0.01	1
19	02 51 54.5	+60 08 26.6	18.196	1.485	2.065	0.6 ± 0.6	1.3 ± 0.1	0.44 ± 0.01	4
20	02 51 58.7	+60 08 05.8	18.760	1.421	2.226	0.7 ± 0.5	1.5 ± 0.1	0.35 ± 0.01	5
21	02 52 11.1	+60 07 15.2	16.047	0.674	1.087	3.8 ± 0.7	4.5 ± 0.8	1.45 ± 0.05	7
22	02 52 15.1	+60 05 18.5	16.692	0.557	1.471	3.1 ± 0.6	1.5 ± 0.2	0.83 ± 0.04	8
23	02 51 54.2	+60 07 43.5	15.384	0.927	1.465	3.2 ± 0.5	0.5 ± 0.0	0.96 ± 0.03	3
24	02 51 59.7	+60 06 39.3	17.693	1.172	1.739	1.5 ± 0.6	1.7 ± 0.2	0.58 ± 0.02	6
25	02 51 52.1	+60 07 10.0	16.677	1.157	1.720	1.7 ± 0.4	0.7 ± 0.1	0.59 ± 0.03	
26	02 52 01.3	+60 06 15.3	18.891	–	2.261	3.0 ± 0.7	1.7 ± 0.1	0.34 ± 0.01	
27	02 51 59.9	+60 05 32.0	18.437	–	1.924	3.3 ± 1.1	2.1 ± 0.5	0.46 ± 0.03	
BRC 11									
28	02 51 32.8	+60 03 54.3	15.967	–	1.431	3.9 ± 0.4	0.9 ± 0.1	0.97 ± 0.03	1
29	02 51 25.6	+60 06 04.8	14.372	0.353	0.860	4.0 ± 0.5	2.7 ± 0.3	2.2 ± 0.08	
BRC 11E									
30	02 52 13.6	+60 03 26.2	20.008	–	2.468	1.0 ± 0.9	2.9 ± 0.3	0.27 ± 0.01	1
31	02 52 14.2	+60 03 11.7	18.291	0.347	2.165	0.8 ± 0.5	1.2 ± 0.1	0.36 ± 0.01	
BRC 13									
32	03 00 51.1	+60 39 36.3	15.917	0.887	–	2.6 ± 0.6	8.0 ± 1.3	1.45 ± 0.04	6
33	03 00 51.6	+60 39 48.9	19.684	–	3.144	2.00 ± 0.6	0.1 ± 0.0	0.19 ± 0.01	7
34	03 00 52.7	+60 39 31.6	18.923	1.371	2.239	0.7 ± 0.6	1.7 ± 0.1	0.34 ± 0.01	10
35	03 00 53.6	+60 40 24.9	13.770	0.492	0.569	5.9 ± 0.6	8.6 ± 0.8	1.72 ± 0.04	11
36	03 00 55.4	+60 39 42.7	15.210	–	0.845	5.6 ± 0.9	8.0 ± 1.4	1.41 ± 0.05	12
37	03 00 56.0	+60 40 26.3	18.169	–	2.508	2.5 ± 0.7	0.1 ± 0.0	0.29 ± 0	13
38	03 00 44.8	+60 40 09.1	19.923	1.974	2.640	0± 0.5	2.2 ± 0.1	0.36 ± 0.00	2
39	03 00 45.3	+60 40 39.5	17.059	1.329	1.695	1.7 ± 0.5	1.0 ± 0.1	0.60 ± 0.02	3
BRC 14									
40	03 01 24.0	+60 30 42.2	17.480	–	1.947	3.9 ± 0.1	0.9 ± 0.0	0.45 ± 0.02	29
41	03 01 24.7	+60 30 09.6	15.586	–	1.379	6.4 ± 0.1	0.7 ± 0.1	0.98 ± 0.08	30
42	03 01 25.6	+60 29 39.0	15.597	–	1.258	4.1 ± 0.1	1.1 ± 0.1	1.20 ± 0.01	31
43	03 01 26.4	+60 30 53.9	15.126	1.068	1.317	3.2 ± 0.1	0.5 ± 0.0	1.10 ± 0.0	32
44	03 01 27.2	+60 30 56.9	18.031	–	1.771	2.9 ± 0.3	2.3 ± 0.2	0.56 ± 0.02	33
45	03 01 27.4	+60 30 39.7	16.498	0.899	1.295	4.2 ± 0.1	2.7 ± 0.3	1.11 ± 0.04	34
46	03 01 29.3	+60 31 13.6	15.511	1.001	1.366	2.8 ± 0.1	0.7 ± 0.1	0.99 ± 0.01	35
47	03 01 34.0	+60 27 45.6	17.503	1.428	1.931	2.9 ± 0.1	0.9 ± 0	0.45 ± 0.01	39
48	03 01 34.4	+60 30 08.5	14.977	–	1.290	5.5 ± 0.1	0.5 ± 0.0	1.19 ± 0.03	40
49	03 01 36.4	+60 29 06.1	16.706	–	1.749	4.8 ± 0.1	0.7 ± 0.0	0.55 ± 0.03	41
50	03 01 37.0	+60 31 00.2	17.326	–	2.031	3.1 ± 0.1	0.7 ± 0.0	0.39 ± 0.01	42
51	03 01 37.1	+60 29 41.2	20.355	–	3.128	0±0.2	0.3 ± 0.0	1.80 ± 0.00	43
52	03 01 43.3	+60 28 51.5	14.893	–	1.047	7.2 ± 0.1	1.4 ± 0.3	1.79 ± 0.11	46

Table 4 – *continued*

S. no.	RA (2000)	Dec. (2000)	V_0 (mag)	$(B-V)_0$ (mag)	$(V-I)_0$ (mag)	$A_V \pm \sigma$ (mag)	Age $\pm\ \sigma$ (Myr)	Mass $\pm\ \sigma$ ($M_\odot$)	ID (Ogura et al. 2002)
53	03 01 50.0	+60 28 50.5	14.444	–	0.773	7.3 ± 0.1	5.6 ± 1.7	1.90 ± 0.18	47
54	03 01 04.2	+60 31 25.3	16.820	–	1.400	3.8 ± 0.1	2.4 ± 0.2	0.94 ± 0.03	1
55	03 01 06.2	+60 30 17.6	17.572	0.763	2.043	3.1 ± 0.1	0.9 ± 0.1	0.29 ± 0.01	3
56	03 01 06.6	+60 30 36.0	19.819	–	2.760	2.5 ± 0.3	1.5 ± 0.3	0.26 ± 0.01	4
57	03 01 07.7	+60 29 21.8	16.119	1.233	1.530	2.2 ± 0.1	0.8 ± 0.0	0.75 ± 0.00	5
58	03 01 11.5	+60 30 46.3	18.474	–	1.981	2.4 ± 0.3	1.8 ± 0.2	0.42 ± 0.04	6
59	03 01 13.4	+60 29 31.9	17.696	–	1.871	4.1 ± 0.1	1.2 ± 0.1	0.48 ± 0.02	8
60	03 01 16.1	+60 29 47.1	17.738	–	2.075	3.4 ± 0.1	0.9 ± 0.0	0.38 ± 0.01	10
61	03 01 17.0	+60 29 23.2	16.532	1.359	1.451	3.4 ± 0.1	1.3 ± 0.1	0.85 ± 0.02	12
62	03 01 20.3	+60 30 02.3	17.826	–	1.723	2.5 ± 0.1	2.1 ± 0.1	0.59 ± 0.01	18
63	03 01 20.6	+60 29 31.7	17.630	0.904	1.592	3.1 ± 0.1	3.1 ± 0.3	0.72 ± 0.02	20
64	03 01 21.2	+60 29 44.3	17.052	–	1.464	3.3 ± 0.1	2.4 ± 0.2	0.85 ± 0.03	23
65	03 01 21.2	+60 30 10.5	18.789	–	2.372	2.2 ± 0.1	1.3 ± 0.0	0.33 ± 0.01	24
66	03 01 32.0	+60 29 36.3	21.235	–	2.460	0.7 ± 0.3	9.0 ± 1.2	0.23 ± 0	
67	03 01 21.9	+60 29 29.5	19.493	–	2.515	1.1 ± 0.9	1.7 ± 0.2	0.28 ± 0.01	
68	03 01 51.4	+60 27 22.7	20.701	–	3.087	1.6 ± 0.9	0.9 ± 0.7	0.17 ± 0.01	
69	03 01 19.4	+60 29 38.9	21.266	–	2.055	0.7 ± 0.2	>30		
70	03 00 47.1	+60 28 53.6	19.343	–	2.273	1.0 ± 0.7	2.3 ± 0.2	0.33 ± 0.01	
71	03 01 20.3	+60 29 49.3	14.746	1.183	1.490	0± 0.4	0.3 ± 0.1	0.89 ± 0.04	
72	03 01 23.5	+60 31 50.6	19.226	–	2.143	1.6 ± 1.2	2.6 ± 0.5	0.36 ± 0.02	
73	03 01 14.1	+60 29 37.4	21.553	–	2.357	0 ± 0.1	>15		
74	03 01 01.1	+60 30 45.2	19.026	–	1.269	2.0 ± 0.1	>30		
75	03 00 58.0	+60 30 13.4	18.655	–	2.253	1.1 ± 0.6	1.4 ± 0.1	0.35 ± 0.01	
76	03 01 00.9	+60 33 26.7	20.402	–	2.989	0.3 ± 1.1	1.8 ± 0.4	0.21 ± 0.01	
77	03 01 02.9	+60 31 22.4	20.978	–	2.961	0.1 ± 1.3	2.8 ± 0.3	0.17 ± 0.02	
78	03 00 57.9	+60 31 21.7	20.406	–	2.961	0.4 ± 0.0	1.8	0.19	
79	03 00 51.8	+60 32 10.8	19.960	–	2.510	0.8 ± 1.3	2.6 ± 0.4	0.27 ± 0.01	
80	03 01 05.2	+60 31 55.4	15.523	1.334	1.727	0.8 ± 0.3	0.1 ± 0.0	0.61 ± 0.01	
BRC 27									
81	07 03 52.8	−11 23 13.2	15.278	0.860	1.326	2.2 ± 0.6	2.0 ± 0.5	1.05 ± 0.09	2
82	07 03 53.8	−11 24 28.4	18.164	–	2.557	1.9 ± 0.6	1.4 ± 0.1	0.29 ± 0.01	4
83	07 03 57.1	−11 24 32.8	16.618	0.920	1.711	2.5 ± 0.4	1.9 ± 0.2	0.60 ± 0.01	7
84	07 04 02.9	−11 23 37.3	15.426	0.642	1.330	3.6 ± 0.6	2.3 ± 0.5	1.03 ± 0.08	8
85	07 04 03.1	−11 23 50.6	15.726	–	1.097	4.5 ± 0.7	11.2±1.1	1.19 ± 0.01	10
86	07 04 04.3	−11 23 55.7	17.151	0.637	1.962	2.5 ± 0.6	1.5 ± 0.2	0.44 ± 0.01	12
87	07 04 04.8	−11 23 39.8	15.620	0.920	1.329	2.7 ± 0.5	3.0±0.5	1.06 ± 0.55	14
88	07 04 05.3	−11 23 13.2	16.378	0.660	1.523	2.7 ± 0.9	3.4 ± 0.8	0.80 ± 0.05	15
89	07 04 06.0	−11 23 58.9	16.791	1.188	1.758	1.4 ± 0.4	1.9 ± 0.2	0.56 ± 0.02	16
90	07 04 06.0	−11 23 15.7	17.568	–	1.800	2.5 ± 0.7	4.5 ± 0.8	0.54 ± 0.03	17
91	07 04 06.5	−11 23 36.2	19.134	–	3.199	1.5 ± 0.6	0.2± 0.0	0.18 ± 0.01	18
92	07 04 06.5	−11 23 16.4	15.700	0.933	1.439	2.4 ± 0.7	1.9 ± 0.3	0.88±0.04	19
93	07 03 52.6	−11 26 16.8	15.064	0.907	1.076	1.8 ± 0.4	5.3 ± 0.4	1.43 ± 0.02	1
94	07 03 55.0	−11 25 14.5	16.887	1.067	1.906	1.9 ± 0.5	1.4 ± 0.1	0.47 ± 0.01	5
95	07 03 56.4	−11 25 41.5	20.435	–	3.039	0 ± 0.9	3.2 ± 1.4	0.14 ± 0.01	6
96	07 04 04.1	−11 26 35.5	20.515	–	3.247	0 ± 0.8	0.9	0.11 ± 0.01	11
97	07 04 08.2	−11 23 54.6	15.644	1.136	1.488	0.3 ± 0.5	1.5 ± 0.1	0.81 ± 0.02	22
98	07 04 08.2	−11 23 09.6	18.795	1.066	2.343	1.5 ± 1.1	3.2 ± 0.5	0.30 ± 0.01	23
99	07 04 09.4	−11 24 38.1	21.053	–	3.792	0 ± 0.6	0.3 ± 0.1	0.10 ± 0.00	24
100	07 04 09.8	−11 23 16.4	14.759	1.039	1.449	0.4 ± 0.3	0.6 ± 0.1	0.85 ± 0.02	25
101	07 04 12.0	−11 24 23.0	19.751	–	3.261	0.6 ± 0.7	0.3 ± 0.0	0.14±0.00	27
102	07 04 13.0	−11 24 03.2	15.189	0.744	0.976	2.4 ± 0.7	9.4 ± 2.5	1.34 ± 0.07	28
103	07 04 13.4	−11 24 55.8	14.604	1.043	1.432	0.9 ± 0.3	0.6 ± 0.1	0.89±0.02	29
104	07 04 14.2	−11 23 17.2	17.430	1.365	1.985	0.2 ± 0.3	1.9 ± 0.1	0.42 ± 0.01	31
105	07 04 14.2	−11 23 37.3	20.043	–	3.034	0.8 ± 0.8	2.9 ± 0.3	0.18 ± 0.01	32
106	07 04 08.4	−11 20 05.3	17.122	1.258	1.909	1.7 ± 0.4	1.7 ± 0.1	0.46 ± 0.01	
107	07 04 03.1	−11 23 27.6	13.749	–	1.209	5.2 ± 0.5	0.6 ± 0.1	1.38±0.06	
108	07 03 54.7	−11 20 11.0	20.425	–	2.709	1.0 ± 1.0	6.3 ± 0.9	0.2 ± 0.01	
109	07 03 52.3	−11 21 01.1	20.808	–	3.117	1.4 ± 0.9	4.0 ± 0.4	0.11 ± 0.01	
110	07 04 12.2	−11 20 20.8	15.657	–	0.567	4.7 ±	>30		
111	07 04 05.8	−11 20 03.8	16.059	–	1.428	4.4 ± 0.6	3.5 ± 1.2	0.92 ± 0.09	
112	07 04 16.8	−11 24 32.4	16.685	0.669	1.545	0.3 ± 0.4	4.7 ± 0.5	0.79 ± 0.02	
113	07 04 15.1	−11 26 22.6	15.313	0.868	1.362	1.9 ± 0.4	1.7 ± 0.2	0.97 ± 0.05	

Table 4 – *continued*

S. no.	RA (2000)	Dec. (2000)	V_0 (mag)	$(B-V)_0$ (mag)	$(V-I)_0$ (mag)	$A_V \pm \sigma$ (mag)	Age $\pm \sigma$ (Myr)	Mass $\pm \sigma$ ($M_\odot$)	ID (Ogura et al. 2002)
114	07 04 19.9	−11 22 22.4	17.050	0.979	1.695	1.2 ± 0.3	3.7 ± 0.4	0.63 ± 0.02	
115	07 04 15.1	−11 23 39.8	18.869	–	2.023	1.8 ± 1.0	8.9 ± 2.4	2.02 ± 0.02	
BRC 38									
116	21 40 26.2	+58 14 24.7	16.917	1.035	1.168	3.3 ± 0.8	>30		1
117	21 40 28.1	+58 15 14.4	16.375	–	1.460	3.8 ± 0.5	11.3 ± 1.9	0.87 ± 0.03	3
118	21 40 31.7	+58 17 55.3	16.082	1.119	1.637	4.2 ± 0.4	3.1 ± 0.4	0.67 ± 0.02	4
119	21 40 37.0	+58 14 38.0	15.288	1.382	1.704	1.4 ± 0.4	0.9 ± 0.0	0.59 ± 0.02	6
120	21 40 37.0	+58 15 03.2	17.644	1.086	2.130	2.5 ± 0.5	3.0 ± 0.3	0.36 ± 0.01	7
121	21 40 41.3	+58 15 11.5	14.673	0.917	1.374	3.4 ± 0.4	1.5 ± 0.2	0.95 ± 0.04	9
122	21 40 41.5	+58 14 25.8	17.398	0.913	1.738	3.2 ± 0.4	12.3 ± 1.8	0.61 ± 0.02	10
123	21 40 44.9	+58 15 03.6	16.921	–	1.653	4.3 ± 0.5	9.5 ± 2.1	0.7 ± 0.04	11
124	21 40 48.0	+58 15 37.8	17.209	1.005	2.441	3.3 ± 0.4	1.3 ± 0.1	0.3	12
125	21 40 49.0	+58 17 09.6	17.374	–	2.035	4.2 ± 0.5	2.9 ± 0.4	0.39 ± 0.02	15
126	21 40 27.4	+58 14 21.5	16.709	0.625	1.530	3.0 ± 0.5	11.9 ± 2.5	0.8 ± 0.02	2
127	21 40 36.5	+58 13 46.2	16.379	1.331	1.902	2.8 ± 0.4	1.5 ± 0.1	0.47 ± 0.01	5
128	21 40 42.7	+58 19 37.6	17.030	–	2.129	4.1 ± 0.4	1.7 ± 0.1	0.37 ± 0.01	
129	21 41 12.0	+58 20 33.7	20.125	–	2.148	1.6 ± 1.2	>30		
130	21 40 45.1	+58 19 50.2	16.277	–	1.421	6.1 ± 0.4	10.2	0.84 ± 0.03	
131	21 39 49.2	+58 14 37.0	20.312	1.930	3.308	0.8 ± 0.4	3.1 ± 0.3	0.13 ± 0.01	
132	21 39 56.4	+58 13 47.7	17.783	1.584	2.274	1.3 ± 0.4	2.5 ± 0.2	0.33 ± 0.01	
133	21 40 21.8	+58 14 45.6	20.447	1.749	3.312	0.7 ± 0.5	3.6 ± 0.5	0.13 ± 0.01	

theoretical isochrones is prone to two kinds of errors; random errors in observations and systematic errors due to the variation between the predictions of different theoretical evolutionary tracks (see e.g. Hillenbrand 2005). The effect of random errors in determination of A_V, age and mass was estimated by propagating the random errors to the observed estimation by assuming normal error distribution and using the Monte Carlo simulations. The use of different PMS evolutionary model gives different age and age spread in a cluster (e.g. Sung, Chun & Bessel 2000). Here in the present study, we have used model by Siess et al. (2000) only for all the BRCs, therefore our age and mass estimations are not affected by the systematic errors. However, the use of different sets of PMS evolutionary tracks will introduce systematic shift in age determination. The presence of binaries may be the another source of error in the age determination. The presence of binary will brighten a star, consequently the CMD will yield a lower age estimate. In the case of equal mass binary, we expect an error of ~50–60 per cent in age estimation of the PMS stars. However, it is difficult to estimate the influence of binaries on mean age estimation as the fraction of binaries is not known. Here, we would like to point out that we are interested mainly in the *relative* ages of the aggregate members, in particular, the spatial differences with respect to the bright rim.

6 STAR FORMATION SCENARIO IN BRC REGIONS

Propagating star formation, where energetic activity of massive stars compresses the surrounding gas and triggers the formation of new generation of stars at the peripheries of H II regions (see e.g. Elmegreen 1998), is quite common in the Galaxy. Some different triggering mechanisms may work in such regions. Briefly, the process which has been frequently supported by the observations is RDI, which takes place in small remnant clouds such as BRCs. The signature of star formation due to RDI is the presence of bright rims and embedded IR sources just inside the dense head. The collect-and-collapse model is another mechanism proposed by Elmegreen & Lada (1977). The signature of this process are the presence of a collected, dense layer adjacent to the ionization front and the presence of massive condensations in it (e.g. Deharveng et al. 2003).

6.1 Small-scale sequential star formation

As for the S^4F hypothesis on the RDI star formation, there has been only qualitative evidence such as an asymmetric distribution of probable TTSs (Ogura et al. 2002) and of properties of NIR excess stars (Matsuyanagi et al. 2006). Very recently, Paper I has quantitatively verified the S^4F hypothesis by using BVI_c photometry of four BRCs. In the present study, we follow the approach as given in Paper I . We have divided the YSOs (Hα stars and NIR excess stars) associated with BRCs into two groups: those lying on/inside and outside of the rims (see Fig. A1). Mean ages and mean A_V values have been calculated for these regions. Some of the stars in Table 4 show ages older than 5 Myr. Since the ages of the associated ionizing sources of BRCs studied here have maximum ages of 4–5 Myr, therefore the TTSs having ages greater than this cannot be expected as products of triggered star formation. We suspect that they may have formed spontaneously in the original molecular cloud prior to the formation of the H II region (see Section 6.3). Some of them may be background stars; larger distances make them look older in the CM diagram. So while calculating the mean ages we have not included those stars. The results are given in Table 5, which shows that in almost all the BRCs the YSOs lying on/inside the rim are younger than those located outside it, whereas the mean A_V is higher on/inside the bright rim than outside it. The only exception for the mean age is BRC 27.

The above results are exactly the same as those obtained in Paper I. Therefore, the present results further confirm the S^4F hypothesis. As in Paper I, we again find a big scatter in the stellar ages for each region of all BRCs in spite of a clear trend of the mean ages. Possible reasons for the scatter include photometric errors, errors in extinction correction, light variation of young stars, their

Table 5. Average age of the YSOs associated with the inside/outside regions of the BRCs.

BRC	Region	No. of stars	Mean age ± std dev (Myr)	Mean Av ± std dev (mag)
			Only Hα stars	
BRC 2	On/inside BR	11	1.0 ± 1.0	3.1 ± 1.4
	Outside BR	-	–	-
BRC 11	On/inside BR	4	1.5 ± 1.1	2.4 ± 1.4
	Outside BR	5	2.1 ± 1.4	2.1 ± 1.4
BRC 13	On/inside BR	3	0.6 ± 0.9	1.7 ± 0.9
	Outside BR	2	1.6 ± 0.9	1.7
BRC 14	On/inside BR	13	1.0 ± 0.7	3.9 ± 1.8
	Outside BR	12	1.6 ± 0.7	3.0 ± 0.6
BRC 27	On/inside BR	11	2.2 ± 1.1	2.3 ± 0.6
	Outside BR	12	2.2 ± 2.5	0.7 ± 0.7
BRC 38	On/inside BR	6	2.1 ± 1.0	3.2 ± 1.1
	Outside BR	1	1.5	2.8
			Hα and NIR excess stars	
BRC 2	On/inside BR	13	1.0 ± 1.0	3.0 ± 1.4
	Outside BR	–	-	-
BRC 11	On/inside BR	8	1.5 ± 0.8	2.3 ± 1.2
	Outside BR	6	2.1 ± 1.3	2.4 ± 1.5
BRC 13	On/inside BR	3	0.6 ± 0.9	1.8 ± 0.9
	Outside BR	2	1.6 ± 0.8	1.7
BRC 14	On/inside BR	15	1.1 ± 0.7	3.6 ± 1.9
	Outside BR	21	1.7 ± 0.8	2.0 ± 1.3
BRC 27	On/inside BR	15	2.3 ± 1.2	2.7 ± 1.2
	Outside BR	14	1.9 ± 1.4	0.7 ± 0.7
BRC 38	On/inside BR	7	2.1 ± 0.9	3.3 ± 1.0
	Outside BR	4	2.7 ± 0.9	1.4 ± 1.0

proper motions, binarity of the stars, etc. Photometric errors and light variation as big as 0.5 mag would affect stellar ages by ~0.25 dex, so they do not seem to be the major reason for the scatter. As to the extinction correction, it probably does not affect the results much again, because in the V_0, $(V - I_c)_0$ CMD the isochrones are nearly parallel to the reddening vector. The adopted evolutionary models and distances of the BRCs causes systematic shifts in ages of the stars, but will not introduce scatters. As discussed in Paper I, we speculate that the proper motions of the newly born stars may be probably the main cause of the scatter.

Since stars inside the rim are often deeply embedded, MIR observations through the *Spitzer Space Telescope* can provide a deeper insight into the embedded YSOs. YSOs occupy distinct regions in the IRAC colour plane; this makes MIR colour–colour diagram a very useful tool for the classification of YSOs. Whitney et al. (2003) and Allen et al. (2004) presented independent model predictions for IRAC colours of various classes of YSOs. Fig. 3 presents [5.8]–[8.0] versus [3.6]–[4.5] colour–colour diagrams for the sources lying in the BRCs 2, 27 and 13/14 regions. The sources within the box represent the location of Class II objects (Allen et al. 2004; Megeath et al. 2004). The sources located around [5.8]–[8.0] = 0 and [3.6]–[4.5] = 0 are foreground/background stars, as well as discless PMS stars (Class III objects). Sources with [3.6]–[4.5] ≥ 0.8 and/or [5.8]–[8.0] ≥ 1.1 have colours similar to those derived from models of protostellar objects with in-falling dusty envelopes (Allen et al. 2004). These are Class 0/I sources.

On the basis of the initial results from the *Spitzer* young cluster survey, Megeath et al. (2004) found a cluster of young stars near the edge of BRC 2 along with a group of Class I sources at the northern apex of the cluster. Table 6 summarizes the IRAC magnitudes of the disc-bearing candidates of BRCs 2, 27 and 13/14, which is available in electronic form only. We reproduce the spatial distribution of the Class I and Class II sources in the BRCs 2 and 27 regions in Fig. 4. The upper panel for BRC 2 shows that the majority of the Class I sources are preferentially located away from the ionization sources (which lies downward in Fig. 4) as compared to the Class II sources. If we divide the BRC into two regions at Dec. ≥ 60° 34.5′, the fraction of Class 0/I sources in the northern region (which is away from the ionizing source) is found to be 0.55 (six Class 0/I and five Class II sources), which is significantly higher than that (0.16, three Class 0/I and 16 Class II sources) in the southern region (towards the ionizing source). This distribution further manifests a small-scale age sequence in the BRC 2 region.

In the cases of BRCs 13 and 14, Allen et al. (2005) reported that the Class I protostars are tightly clustered on the edge of the molecular clouds, coincident with the interface of the ionized and molecular gas, whereas the Class II stars are more widely distributed. The distribution of YSOs detected using the IRAC data is reproduced in Fig. 5, where again Class 0/I sources are found concentrated inside the BRCs, which is in accordance with the S^4F hypothesis. In the IC 1396N = BRC 38 region, Getman et al. (2007) found an elongated spatial distribution of YSOs with the youngest stars (Class 0/I) deeply embedded inside the cloud and relatively older stars aligned towards the exciting star, which again supports propagation of small-scale triggered star formation in that region.

6.2 Indication of global triggered star formation

BRCs are considered to be a sort of remnants originated from dense part (cores) in an inhomogeneous giant molecular cloud. So, if the original cloud was big, the resultant BRC could have undergone a series of RDI events, leaving an elongated distribution of young stars; the distribution of such YSOs and its morphological details could be used to probe the star formation history in the OB

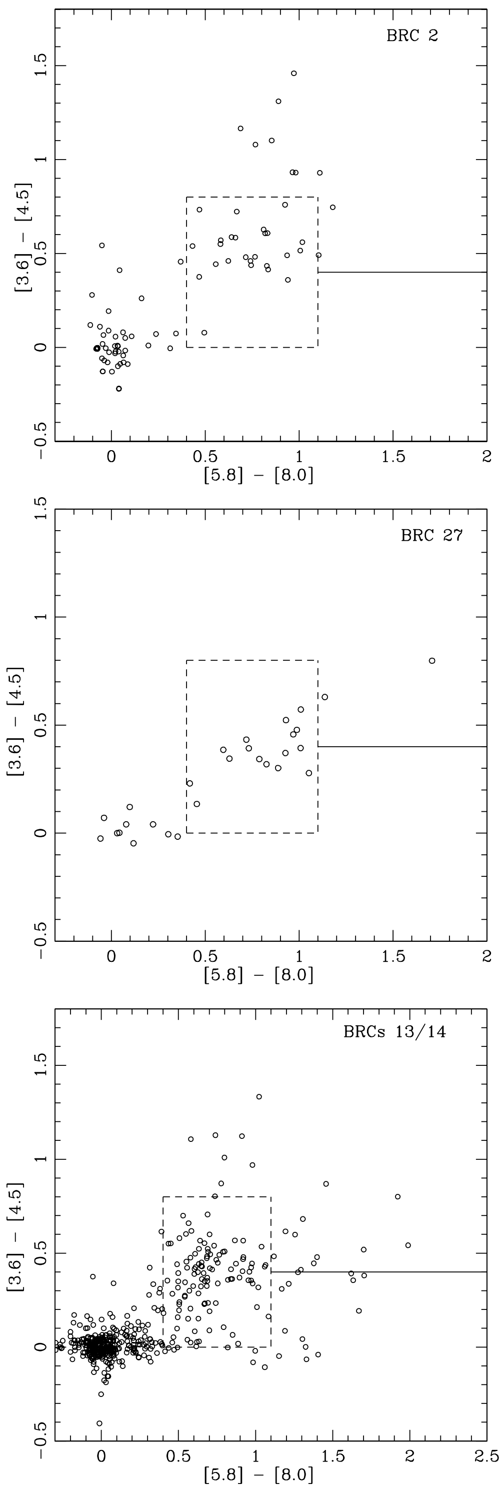

Figure 3. IRAC colour–colour diagrams for YSOs in BRCs 2, 27 and 13/14. The sources lying within the box are Class II sources. The sources located around [5.8]–[8.0] $\sim$ 0 and [3.6]–[4.5] $\sim$ 0 are the field/ Class III stars. Sources with [3.6]–[4.5] $\geq$ 0.8 and/or [5.8]–[8.0] $\geq$ 0.8 represent Class 0/I sources. The horizontal continuous line shows the adopted division between Class I and Class I/II sources (see Megeath et al. 2004).

association. With this expectation, we have searched for NIR excess stars by using 2MASS PSC in the whole H II regions where the studied BRCs are located. Figs A2–A5 show spatial distribution of NIR excess stars in the IC 1848W, IC 1848E, CMaR1 and IC 1396 regions which contain BRCs 11NE, 13/14, 27 and 38, respectively. These figures are available in electronic form only. Figs 6–8 show radial variation of $\Delta(H - K)$ and A_V, for the stars located within the strip shown in Figs A2–A4. The NIR data along with $\Delta(H - K)$ and A_V values are given in Table 7, which is available in electronic form only.

Fig. A2 shows that the NIR excess stars are aligned loosely towards the direction of BRC 11NE from the cluster IC 1848W which contains the ionizing sources (HD 17505, O6 V; HD 17520, O9V) of the H II region. A very recent study (while the present study was in the reviewing process) based on *Spitzer* observations by Koenig et al. (2008) also shows a nice alignment of Class II stars towards the direction of the BRC 11NE region from the ionizing source(s) (see their fig. 10). Figs 6(a) and (b) show radial variation of $\Delta(H - K)$ and A_V, for the stars in the BRC 11NE region located within the strip shown in Fig. A2, as a function of radial distance from HD 17505. $\Delta(H - K)$ is defined as the horizontal displacement from the middle reddening vector (see Fig. 1). The distribution of the NIR excess $\Delta(H - K)$ values shows an increasing trend as we move towards the BRC 11NE region. For the whole sample shown in Fig. 6(a), the Kendall's tau test gives a positive correlation at a confidence level of about 85 per cent. The two extreme points at radial distance ~28 arcmin have small $\Delta(H - K)$ values with small A_V (0.24 and 0.84) values. We presume that these sources are not embedded inside the rim and lying on the outer region of the cloud. The two stars at radial distance ~5 and ~9 arcmin shows relatively higher value of $\Delta(H - K)$ in comparison to nearby stars. Exclusion of these four points gives a probability of ~97 per cent for a positive correlation between radial distance and $\Delta(H - K)$. Table 8 summarizes the results of the correlation analysis using the Kendall's tau test.

On the basis of the pressure of the IBL and that of the molecular cloud, Thompson et al. (2004) have concluded that the cloud is in pressure balance with the exterior ionized gas and photoionization-induced shocks are propagating in the cloud. They also concluded that overall morphology of the cloud is similar to that predicted by RDI models (Bertoldi 1989; Lefloch & Lazareff 1994). They have also estimated the duration over which the BRC 11NE region might have been exposed to the UV flux. Assuming that the rims are located at a distance of ~22 pc from the ionizing sources, an ionization front expanding into a medium of homogeneous density at a speed of 11.4 km s^{-1} will take about 1.5 Myr to reach the rims. The mean age of the YSOs (Hα stars and NIR excess stars) associated with BRC 11NE (both inside and outside the bright rim) is found from Table 4 to be 1.7 $\pm$ 1.0 Myr. Thus, the sum of these two values yields a time-scale of ~3.2 Myr, which is comparable to the MS lifetime (~4.0 Myr) of HD 17505 (Lang 1992; Schaller et al. 1992). The above facts seems to support the triggered star formation scenario in the IC 1848W region.

Fig. A3 shows that the distribution of the NIR excess stars in the IC 1848E region. We see they are aligned beautifully from the vicinity of the O7 star HD 18326 to the direction of BRC 14. A more impressive alignment of the Class II sources can be seen in fig. 7 of Koenig et al. (2008). This spatial distribution of NIR excess stars resembles that in NGC 1893, where a similar nice distribution of NIR excess stars is noticed from the centre of the cluster containing several OB stars to the direction of the cometary globules Sim 129 and 130 (see fig. 22 of Sharma et al. 2007). In the case of NGC 1893, evidence for triggered star formation due to RDI is also found. In Fig. 7(a) (upper panel), we plot the amount of NIR excess $\Delta(H - K)$ for the stars shown in Fig. A3 as a function of radial distance from the centre of the cluster. Fig. 7(a) manifests

Table 6. IRAC photometric magnitudes of the disc-bearing candidates in BRCs 2, 27 and 13/14. The complete table is available in electronic form only (see Supporting Information).

RA (J2000)	Dec. (J2000)	[3.6]	e[3.6]	[4.5]	e[4.5]	[5.8]	e[4.5]	[8.0]	e[8.0]	IRAC type
BRC 2										
00 04 14.69	+68 32 49.8	11.899	0.033	10.97	0.03	10.095	0.052	8.985	0.028	0/I
00 03 57.27	+68 33 24.4	12.231	0.038	11.74	0.042	11.100	0.087	9.996	0.075	0/I
00 04 03.83	+68 32 49.6	13.316	0.064	12.57	0.062	11.749	0.123	10.57	0.117	0/I

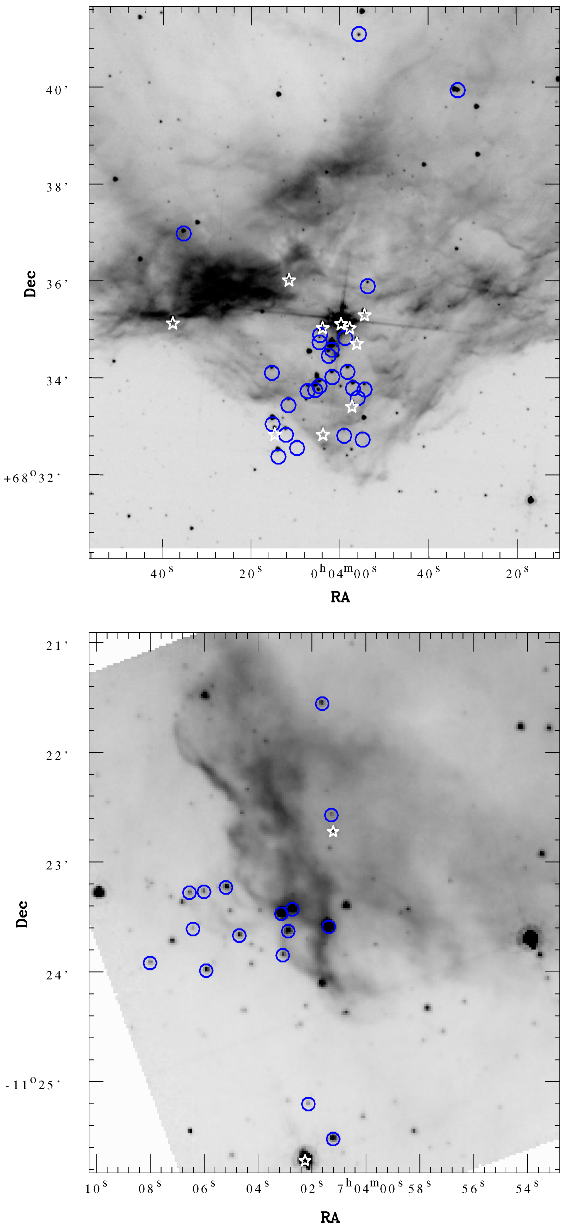

Figure 4. Spatial distribution of Class 0/I sources (star symbols) and Class II sources (open circles) in the BRC 2 (upper panel) and BRC 27 (lower panel) regions.

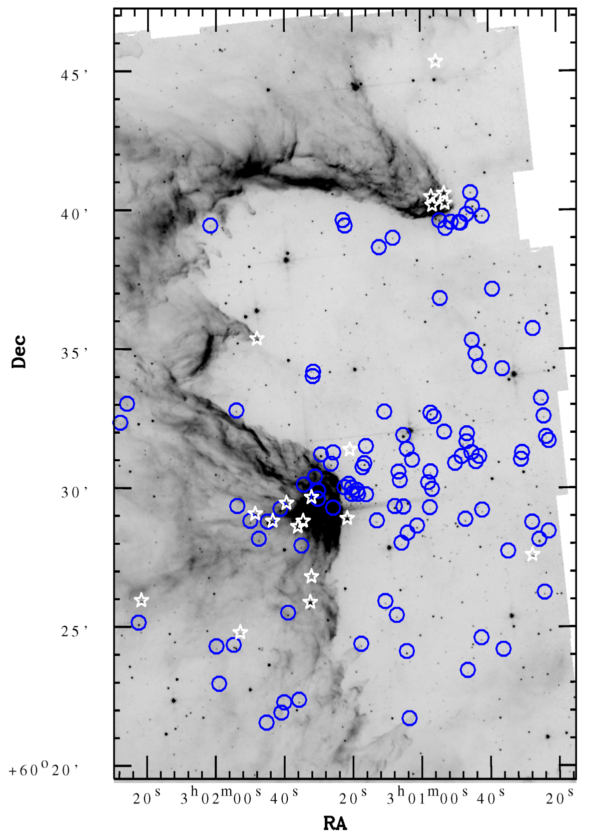

Figure 5. Spatial distribution of Class 0/I sources (star symbols) and Class II sources (open circles) in the BRCs 13 and 14 region identified in the *Spitzer*/IRAC data.

an increase in NIR excess near BRC 14. A similar trend is noticed for the spatial distribution of A_V (Fig. 7b). Kendall's tau test yields a positive correlation for the radial variation of $\Delta(H - K)$ and A_V at a confidence level of better than 99.9 per cent. As discussed in Matsuyanagi et al. (2006), these features indicate that stars located near BRC 14 should be younger than the rest of the stars.

In Fig. A3, a loose clustering is also clearly visible around HD 18326. To our knowledge, this clustering has not been designated so far as a known cluster.[1] $J/(J - H)$ CM diagram of the cluster region yields an age of ∼2 Myr. This cluster will be studied in detail in a forthcoming paper. On the other hand, the mean age of the YSOs associated with BRCs 13 and 14 (again, both inside and outside of the rims) is derived from Table 4 to be 1.0 ± 0.9 Myr and 1.5 ± 0.9 Myr, respectively, which are younger than the age of the cluster. Recently Nakano et al. (2008) reached the same conclusion, obtaining the ages of 4 and 1 Myr for a groups of Hα emission stars around HD 18326 and that near eastern edge of the H II region, respectively. This again indicates that the star formation in the BRCs 13/14 region is triggered by the O star in the cluster

[1] In a very recent study based on *Spitzer* observations, Koenig et al. (2008) have also identified this cluster.

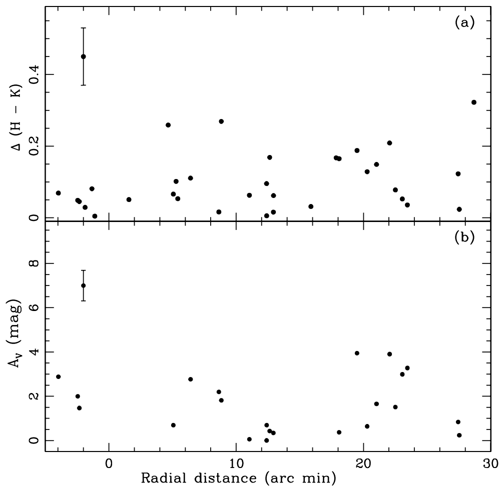

Figure 6. Variation of (a) NIR excess $\Delta(H-K)$ and (b) A_V for the stars within the strip shown in Fig. A2 as a function of distance from HD 17505 towards BRC 11 region. Average error bar is shown at the upper-left corner of the plot.

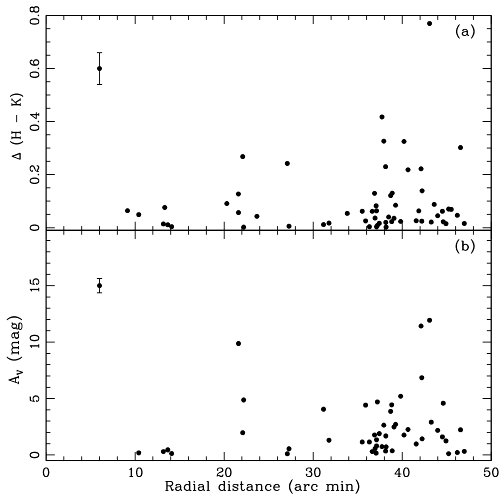

Figure 8. Variation of (a) NIR excess $\Delta(H-K)$ and (b) A_V for the stars within the strip shown in Fig. A4 as a function of distance from the probable ionizing source (HD 53974) of the CMaR1 region. Average error bar is shown at the upper-left corner of the plot.

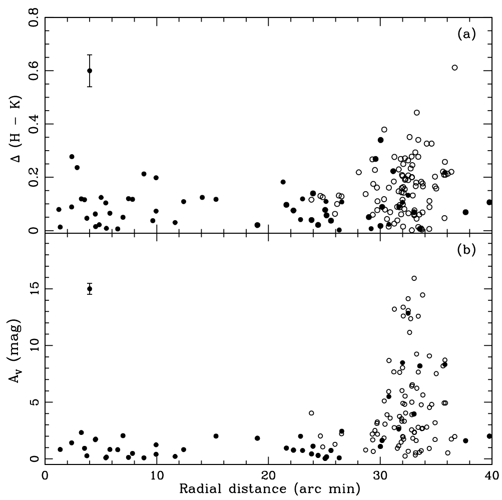

Figure 7. Variation of (a) NIR excess $\Delta(H-K)$ and (b) A_V as a function of the distance from HD18326 towards BRC 14. Filled and open circles represent the data taken from the 2MASS catalogue and Matsuyanagi et al. (2006), respectively. Average error bar is shown at the upper-left corner of the plot.

region. Thus, all the above-mentioned evidences clearly support a series of RDI processes which took place in the past starting from the vicinity of the O star.

The spatial distribution of the NIR excess stars in the BRC 27 region is shown in Fig. A4. Assuming that B0.5IV (HD 53974; marked as '2') and B1V (HD 54025; marked as '1') stars are the ionizing sources for the BRC 27 region, the $\Delta(H-K)$ and A_V distribution for the sources lying within the strip marked in Fig. A4 as a function of radial distance from HD 54025 is shown in Fig. 8, which indicates relatively higher NIR excess and A_V near the BRC 27 region. The Kendall's tau test for the entire sample indicates a positive correlation between radial distance and $\Delta(H-K)$ and A_V at a confidence level of ∼80 and ∼95 per cent, respectively. The sources having radial distance >43 arcmin show small value of A_V as well as $\Delta(H-K)$ as compared to the sources lying around 40–41 arcmin. We presume that these sources are not embedded inside the rim and are lying on the outer periphery of the cloud. Exclusion of these points gives a probability of ∼98 per cent or better and 99.9 per cent for a positive correlation between radial distance and $\Delta(H-K)$; and A_V, respectively. If the B1V/ B0.5 IV star(s) is (are) actually the ionizing source(s) for the region, the maximum MS lifetime of the star(s) is ∼10 Myr (Lang 1992; Schaller et al. 1992), whereas the mean age of the YSOs associated with BRC 27 is estimated as 2.1 ± 1.3 Myr, which is not in contradiction with that star formation in the BRC 27 region may be initiated by the UV radiation from these star(s).

Sicilia-Aguilar et al. (2004) have shown that in the case of the Tr 37/ IC 1396 Globule region, CTTSs are found to be aligned towards the direction of IC 1396 Globule from the ionizing source, HD 206267 (O6). Sicilia-Aguilar et al. (2005) found that most of the younger (∼1 Myr) members appear to lie near or within the IC 1396 Globule. They concluded that it can be indicative of the triggered star formation. Fig. A5 shows distribution of NIR excess stars in the Tr 37/IC 1396 Globule/BRC 38 region, where they seem to align loosely towards the direction of IC 1396 Globule and BRC 38. Their radial distribution of NIR excess $\Delta(H-K)$ and A_V does not show any trend, however. By using the ages of the YSOs near IC 1396 Globule given by Sicilia-Aguilar et al. (2005) we obtained their mean age of ∼1.8 ± 1.1 Myr, whereas for the YSOs near BRC 38 the mean age is estimated from Table 4 to be ∼2.2 ± 0.9 Myr. The upper main-sequence turn-off age of Tr 37 is found to be ∼3 Myr (Contreras et al. 2002). Thus the aligned distribution of YSOs from the ionizing source HD 206267 towards IC 1396 Globule and BRC 38 and their younger age as compared to the central cluster Tr 37 suggest a triggered star formation scenario in the region.

We conclude that the global distribution of YSOs, their radial distribution of the amount of NIR excess $\Delta(H-K)$ as well as of A_V in each H II region studied here clearly show evidence that a series of RDI processes proceeded in the past from near the central O star(s) towards the peripheries of the H II region.

6.3 Star formation inside 'A'-type BRCs

The *Spitzer*/IRAC data on BRC 2, BRC 13 and BRC 14 manifest that the Class 0/I sources are concentrated inside the rim. The SCUBA

Table 7. *J*, *H* and *K* magnitudes of the sources used in the analysis (cf. Section 6.2). The complete table is available in electronic form only (see Supporting Information).

RA (J2000)	Dec. (J2000)	2MASS name	J ± eJ (mag)	$H \pm eH$ (mag)	$K \pm eK$ (mag)	Q flag	C flag	A_V (mag)	$\Delta(H-K)$ (mag)	2MASS/Matsuyanagi et al. 2006
IC 1848W										
02 51 12.63	+60 24 00.1	02511262+6024000	13.719 ± 0.050	12.912 ± 0.051	12.361 ± 0.035	AAA	000	0.00	0.05	2MASS
02 51 24.86	+60 21 40.2	02512485+6021402	14.305 ± 0.038	13.545 ± 0.043	13.017 ± 0.031	AAA	000	0.00	0.05	2MASS
02 51 12.27	+60 25 51.3	02511226+6025512	15.955 ± 0.086	15.189 ± 0.103	14.630 ± 0.099	AAA	c00	0.00	0.08	2MASS

Table 8. Correlation between radial distance and $\Delta(H-K)$, A_V. The probability P(0) indicates that no correlation is found with the generalized non-parametric Kendall's tau statistics.

Radial distance from the ionizing source (arcmin)	$P(0)$ $\Delta(H-K)$	$P(0)$ A_V	Comment
	BRC 11		
5–30	0.150	–	
5–30	0.026	–	Excluding outliers (see text)
	BRC 14		
0–40	<0.00	<0.00	
	BRC 27		
0–48	0.230	0.04	
0–43	0.025	0.001	(see text)

imaging survey of submillimeter continuum emission from BRCs by Morgan et al. (2008) has shown that the embedded cores are likely to contain Class 0 protostars. On the basis of combination of the observed submillimeter flux excess and high dust temperature, they concluded that star formation may be ongoing within the BRCs. They have further concluded that the majority of the sources have $L_{\mathrm{bol}} > 10\,\mathrm{L}_{\odot}$, indicating that the sources are intermediate to high-mass stars. Some of the higher luminosity sources (e.g. in BRCs 13 and14) may be protoclusters. The *Spitzer*/IRAC data manifest that in fact these two BRCs host a protocluster (cf. Fig. 6).

Morgan et al. (2008) did not find evidence for interaction of the external ionization field with the star formation inside 'A'-type BRCs (for the morphological types of BRCs we refer to SFO91) and concluded that the star formation in these clouds is not subjected to the RDI process. The present work includes four BRCs of the 'A' type, namely BRCs 2, 14, 27 and 38 (as for BRC 38, see Section 8) and provides strong evidence for star formation due to RDI occurring in BRCs, however. As we have seen in Section 6.1, BRCs 2, 14 and 38 show such age gradients that stars located on/inside the rim are younger than those located outside it, i.e. towards the ionizing source, evidencing the most recent RDI phenomenon. In addition, our results in Section 6.2 as well as recent study based on *Spitzer* observations by Koenig et al. (2008) manifest a nice, global alignment of NIR excess stars in IC 1848E from the O7 star HD 18326 to BRCs 13 and 14. The spatial distribution of Hα emission stars found by Nakano et al. (2008) also revealed a similar alignment. Thus, the ages of the YSOs and their spatial distribution in the region clearly support a series of RDI processes which have been taking place in the past until very recently. These results do not support the notion of Morgan et al. (2008) that star formation in/around 'A'-type BRCs is not subjected to the RDI triggering process.

7 EVOLUTION OF Hα EW AND DISC OF T-TAURI STARS

Hα emission and IR excess are important signatures of young PMS stars. These signatures in CTTSs indicate the existence of a well-developed circumstellar disc actively interacting with the central star. Strong Hα emission (EW > 10 Å) in CTTSs is attributed to the magnetospheric accretion of the innermost disc matter on to the central star (Edwards et al. 1994; Hartmann, Hewett & Calvet 1994; Muzerolle, Calvet & Hartmann 2001, and references therein). On the other hand, the weak Hα emission (EW < 10 Å) in weak-line TTSs (WTTSs), which lack discs (or, at least inner discs), is believed to originate from their chromospheric activity (e.g. Walter et al. 1988; Mart'in 1998). In 1990s, a large number of WTTSs were found in and over wide areas around T associations by X-ray surveys with *ROSAT*, which aroused active studies on the nature of the so-called dispersed WTTSs. For a detailed discussions on this topic, we refer to Caillault et al. (1998). As for the relation of the WTTS to the CTTS, the 'standard model' (Kenyon & Hartmann 1995) postulates that the latter evolves to the former by losing the circumstellar disc (or, at least its inner part). Actually analysis of the age distribution derived from the HR diagram of, e.g. the Taurus region indicated that the WTTSs are systematically older than the CTTSs, but the statistical significance was low (Kenyon & Hartmann 1995; Hartmann 2001; Armitage, Clarke & Palla 2003).

On the other hand, there also have been many observations which claimed that the CTTS and the WTTS are coeval and have indistinguishable stellar properties (e.g. Walter et al. 1988; Lawson, Fiegelson & Huenemoerder 1996; Gras-Vel'azquez & Ray 2005). From the analyses of the HR diagram of the CTTSs and WTTSs in Chamaeleon I, Lawson et al. (1996) concluded that some stars may be born even almost discless or lose the disc at very early stages (age < 1 Myr). However, in order to explain the coexistence and approximate coevality of CTTSs and WTTSs in a star-forming region, it is usually postulated that YSOs display a wide range of disc masses and their accretion activity and/or the dispersal of the disc takes place in a correspondingly wide range of time-scales (Furlan et al. 2006; Bertout et al. 2007). Based on L-band surveys of clusters of various ages, Haisch, Lada & Lada (2001) reached the quantitative conclusion that the disc fraction is initially very high ($\geq$80 per cent) and that one-half of the stars lose their discs in $\sim$3 Myr and almost all in $\sim$6 Myr. Armitage et al. (2003) obtained similar results that around 30 per cent of stars lose their discs within 1 Myr, while the remainder have disc lifetimes that are typically in the 1–10 Myr range. Recently, Bertout et al. (2007), by using new parallaxes for CTTS and WTTS in the Taurus–Auriga T association, concluded that their observed age and mass distribution can be explained by assuming that a CTTS evolves into a WTTS when the disc is fully accreted by the star.

In the present work, we have derived the ages of 93 Hα emission stars, hence we can study the evolution of the Hα emission activity in TTSs. The advantage of our sample in addressing this issue is that the stars are spatially, i.e. three-dimensionally, very close to each other, so there should be no problem of the distance difference, contrary to the extended T associations. The Hα EWs are taken from Ogura et al. (2002); however, the values reported as EWs in their table 5 are values in pixels. To convert these values into Å we multiply the reported values by a factor of 3.8 (see Ikeda et al. 2008).

In Fig. 9, we plot the EWs of Hα emission stars as a function of age to explore possible evolutionary trends. Although, the dispersion around younger side is quite large, still in general there seems to be a decreasing trend in EW with the age. Here, it is worthwhile to mention that a rather similar trend in the EWs of Hα emission line of HAe/Be stars is reported by Manoj et al. (2006). The distribution of EWs in Fig. 9 indicates that the accretion activity in the TTSs associated with BRCs drops substantially by 5 Myr. In Fig. 9, there seems to be a small group of Hα emission stars having far larger ages ($\geq$5 Myr) and a relatively elevated level of EWs. The masses of these stars lie in the range $0.6 \geq M/\mathrm{M}_{\odot} \geq 1.9$, whereas the majority of the YSOs having age $\leq$5 Myr have masses in the range $0.1 \geq M/\mathrm{M}_{\odot} \geq 1.2$. If we take their ages at their face values, they presumably are not products of triggering. Since the ages of

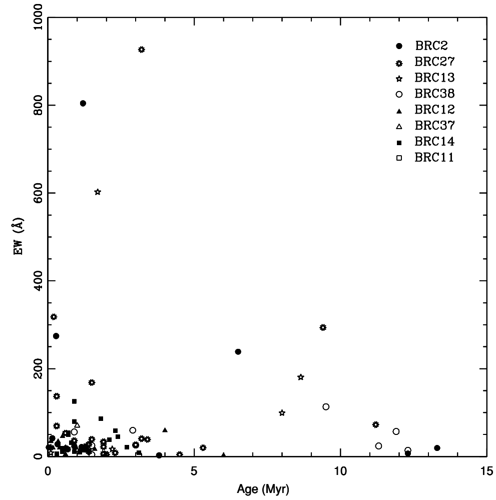

Figure 9. EWs of Hα emission stars in our sample as a function of stellar ages.

the ionizing sources of BRCs studied here have maximum age of 4–5 Myr, stars having ages greater than $\sim$5 Myr cannot be expected as results of triggered star formation, but must have formed spontaneously prior to the formation of the H II region. The stars with ages $\geq$5 Myr seem to be born with large disc masses and spent a substantial part, say, half of their ages unexposed to UV radiation from O stars, the long lifetime of their accretion activity may be understood. Johnstone et al. (2004) have reported that the far-UV radiation from nearby massive star(s) may cause photoevaporation of YSO discs resulting in short ($\sim$10^6 yr) disc lifetimes. However, Fig. A1, where these stars are marked with crosses, shows that they are located both inside and outside the bright rims mixed with Hα stars of younger ages. So, their origin remains a mystery. But in the case of BRC 38, which contributes four to this group of altogether eleven stars, Getman et al. (2007) recognized, apart from young stars associated with the BRC, an older population of PMS stars dispersed in IC 1396. We suspect the above four stars may belong to this population and formed in the original molecular cloud prior to the formation of HD 206267. In Fig. A1, they look concentrated along the bright rim, but note that the Hα survey by Ogura et al. (2002) is limited down to +58 13 35, which is only a few arcmin south of the bright rim. Here, it is worthwhile to mention that in the case of cluster Tr 37 (age 1–5 Myr), Sicilia-Aguilar et al. (2005) have found a few stars having age >5 Myr. They pointed out that in some clusters intermediate-mass stars seem older than low-mass stars and this effect seems to be related to a problem defining the birth line for intermediate-mass stars (Hartmann 2003).

Fig. 10 shows the cumulative distribution of CTTSs (EW $\geq$ 10 Å) and WTTSs (EW $<$ 10 Å) (for stars having age $\leq$5 Myr) as a function of age. Fig. 10 manifests that CTTSs are relatively younger than WTTSs. A Kolmogorov–Smirnov test confirms the statement that the cumulative distributions of CTTSs and WTTSs are different at a mean confidence level of $\sim$70 per cent with minimum and maximum confidence level (obtained using the Monte Carlo simulations) of $\sim$55 per cent and $\sim$90 per cent, respectively. This result is in agreement with that of Bertout et al. (2007) for the Taurus–Auriga T association, that WTTSs are older than CTTSs and CTTSs evolve into WTTSs. In Fig. 11, we plot cumulative age distribution of Hα emission stars (EW $\geq$ 10 Å) and of NIR excess stars. Fig. 11, at a mean confidence level of $\sim$98 per cent (with a minimum and maximum confidence level of $\sim$92 and $\sim$99.4 per cent), indicates

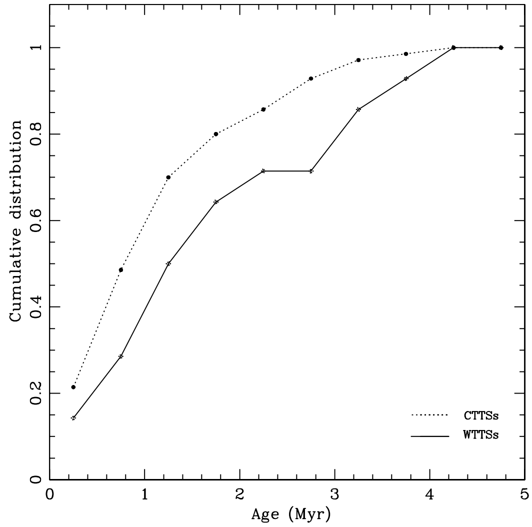

Figure 10. Cumulative distributions of CTTSs and WTTSs in our sample as a function of stellar age.

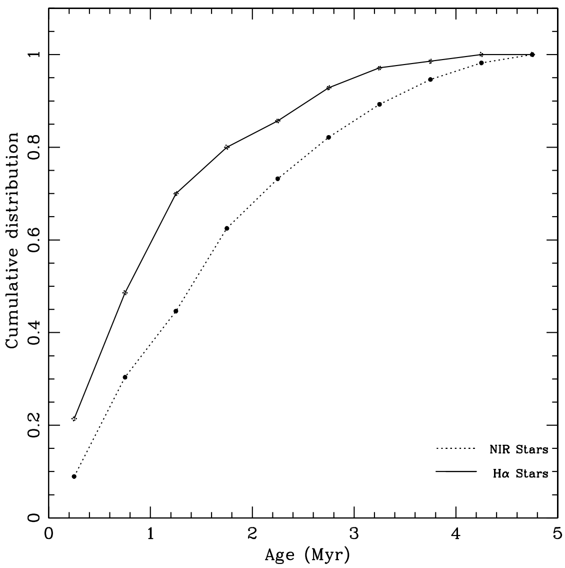

Figure 11. Cumulative distributions of Hα emission and NIR excess stars in our sample as a function of stellar age.

that YSOs exhibit NIR excess for a relatively longer time as compared to accretion activity. Although our sample is small and the age span is very short, the obtained CTTS fraction (from Tables 3 and 4) in BRCs seems to follow the trend of TTSs in the Taurus region as given by Armitage et al. (2003).

8 MASS FUNCTION OF BRC AGGREGATES

The initial mass function (IMF) is an important tool to study the star formation process. Morgan et al. (2008), using SCUBA observations, have estimated the masses of 47 dense cores within the heads of 44 BRCs. They concluded that the slope of the MF of these cores is significantly shallower than that of the Salpeter MF. They also concluded that it depends on the morphological type of BRCs (for the morphological description of BRCs, we refer to SFO91): 'A'-type BRCs appear to follow the mass spectrum of the clumps in the Orion B molecular cloud, whereas the BRCs of the 'B' and 'C' types have a significantly shallower MF.

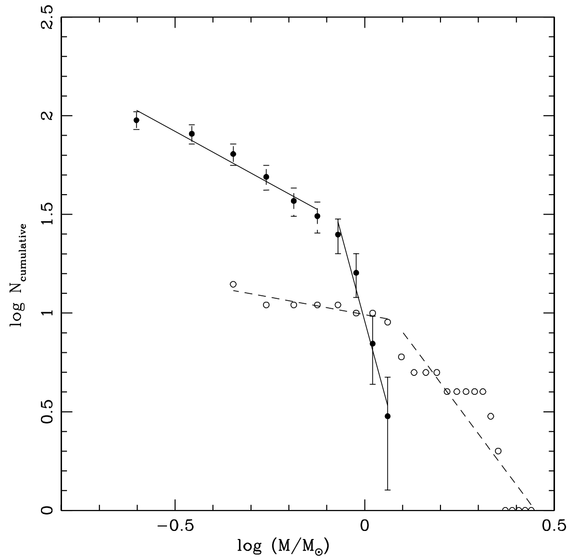

Figure 12. CMF of YSOs in the seven BRCs (filled circles). Error bars represent $\pm\sqrt{N}$ errors. Open circles represent the CMF for the cores by Morgan et al. (2008).

It would be worthwhile to compare the MF of protostars given by Morgan et al. (2008) with that of BRC aggregates. In Fig. 12, we plot cumulative mass function (CMF) of the YSOs in seven BRCs, namely BRCs 2, 11NE, 12, 13, 14, 27 and 38, in the mass range of $0.2 \le M/\mathrm{M}_{\odot} \le 1.2$. Here we have supplemented the present data with the data of BRC 12, taken from Paper I, because among the present sample of BRCs there are fewer number of BRCs of type 'B' than those of type 'A'. The CMF of the dense cores by Morgan et al. (2008) is also plotted for comparison.

It is interesting to note that both CMFs show a roughly similar shape with a break in power law. Obviously, a detailed comparison manifests differences. In the case of the YSOs we find a break in the slope of the CMF at $\sim 0.8\,\mathrm{M}_{\odot}$. In the mass range $0.8 \le M/\mathrm{M}_{\odot} \le 1.2$, the slope of the CMF is -7.1 ± 0.9 and it becomes shallower (-1.0 ± 0.1) for masses $0.2 \le M/\mathrm{M}_{\odot} \le 0.8$, whereas the CMF of the cores can be represented by a power law with a shallower slope of -0.4 ± 0.1 in the mass range $0.4 \le M/\mathrm{M}_{\odot} \le 1.2$. The core CMF becomes steeper for masses $\ge 1.2\,\mathrm{M}_{\odot}$ (slope $= -2.6 \pm 0.3$). Morgan et al. (2008) have reported that their sample is complete down to $0.5\,\mathrm{M}_{\odot}$. Our sample towards lower mass may be affected by incompleteness, however the correction due to incompleteness will further steepen the CMF slope of the YSOs. The shallower CMF slopes in the case of dense cores than those for YSOs indicates that the star formation in the next sequence/ generation favours formation of relatively massive stars.

If the star formation within the BRCs depends on morphology of the clouds, as suggested by Morgan et al. (2008), it would be interesting to study the CMF of YSOs by separating the target BRCs on the basis of the morphology of BRCs. Here, we assign type A to BRC 38 rather than type B given in SFO91. BRC 11NE, which is not included in SFO91, is classified as type B. In Fig. 13, we plot the CMFs of the YSOs in 4 'A'-type BRCs, namely BRCs 2, 14, 27 and 38, and of those in 3 'B/C'-type BRCs, namely BRCs 11NE, 12 and 13. In the YSO mass range $0.2 \le M/\mathrm{M}_{\odot} \le 0.8$ the slope of the CMF for the 'B/C'-type BRCs is found to be -1.5 ± 0.2 which is steeper than that (-0.9 ± 0.1) obtained for 'A'-type BRCs. This is in contradiction with the results reported by Morgan et al. (2008). They reported a shallower MF slope for 'B/C'-type

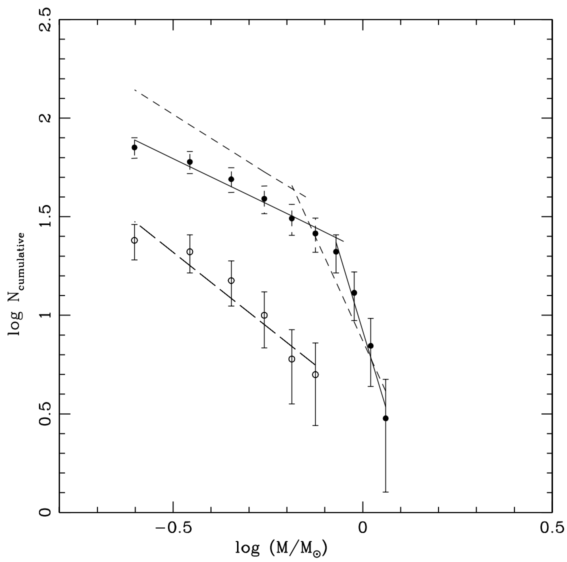

Figure 13. CMF of the 'A'-type (filled circles) and 'B/C'-type BRCs (open circles). Error bars represent $\pm\sqrt{N}$ errors. The CMF for the standard MF is shown by short dashed lines (see the text).

BRCs in comparison to that of 'A'-type BRCs (see their fig. 11); however, a close inspection of their fig. 11 manifests that in the mass range $0.5 \leq M/\mathrm{M}_{\odot} \leq 3.0$, the MF slope of the cores of 'A'-type BRCs is definitely shallower than that for 'B/C'-type BRCs. This suggests that 'A'-type rims, in the mass range $0.4 \leq M/\mathrm{M}_{\odot} \leq 1.2$, appear to follow a MF that is more biased towards formation of relatively massive stars in comparison to that in case of 'B'- and 'C'-type BRCs.

In Fig. 13, we have also plotted the CMF generated for a sample aggregate having an average Galactic IMF, i.e. $\Gamma = -1.35$ for $0.6 \leq M/\mathrm{M}_{\odot} \leq 1.2$, and $\Gamma = -0.3$ for $0.2 \leq M/\mathrm{M}_{\odot} \leq 0.6$ (Kroupa 2001, 2002). The slope of the CMF in the mass range $0.2 \leq M/\mathrm{M}_{\odot} \leq 0.6$ comes out to be $\sim -1.1 \pm 0.1$, which is close to the slope of the CMF (-0.9 ± 0.1) of the YSOs ($0.2 \leq M/\mathrm{M}_{\odot} \leq 0.8$) in the 'A'-type BRCs. Whereas, the CMF slope for YSOs in the 'B/C'-type BRCs is significantly steeper (-1.5 ± 0.2) than the standard MF. This suggests that in the mass range $0.2 \leq M/\mathrm{M}_{\odot} \leq 0.8$ the YSOs in 'A'-type BRCs follow the standard form of MF, whereas aggregates in 'B/C'-type BRCs is more biased towards relatively less massive objects. We have also estimated the effect of errors on estimation of MF. The results are given in Table 9 which indicate an insignificant effect on the MF slopes.

Table 9. MF of BRC aggregates. The maximum and minimum value of the slopes are estimated by propagating the random errors using the Monte Carlo simulations.

Mass range ($\mathrm{M}_{\odot}$)	Mean value of the slope	Maximum value of the slope	Minimum value of the slope
All BRCs			
0.2–0.8	-0.97 ± 0.14	-0.99 ± 0.15	-0.95 ± 0.15
0.8–1.2	-7.08 ± 0.89	-8.17 ± 0.86	-6.40 ± 0.62
A-type BRCs			
0.2–0.8	-0.92 ± 0.09	-0.96 ± 0.10	-0.87 ± 0.11
0.8–1.2	-6.40 ± 0.78	-7.60 ± 0.74	-5.60 ± 0.55
B/C-type BRCs			
0.2–0.8	-1.53 ± 0.20	-1.63 ± 0.20	-1.20 ± 0.17

9 CONCLUSIONS

On the basis of the present optical and NIR analysis of six BRC aggregates, we reached the following conclusions.

We estimated the ages of individual stars associated with BRCs from the reddening-corrected V_0, $(V - I_c)_0$ CM diagrams. By comparing the average ages of the stars on/inside and outside the bright rim, we again found quantitative age gradients in almost all the studied BRCs (the only exception being BRC 27), although the number of the sample stars are small and their age scatters are large. The results are quite similar to the results reported in Paper I. In addition, the youngest objects, obtained from *Spitzer* MIR data, are found to be deeply embedded inside the BRCs, supporting the above conclusion. These results further confirm S^4F hypothesis.

The distribution of NIR-excess stars in the studied H II regions indicates that they are aligned from the ionizing source to the BRC direction. The age indicators, viz. IR excess ($\Delta(H - K)$) and A_V as well as the age itself of the YSOs manifest an age gradient towards the ionizing source. This global distribution indicates that a series of triggered star formation took place in the past from near the central O star(s) towards the peripheries of the H II region.

It is found that the EW of Hα emission in TTSs associated with the BRCs decreases with age. We found some Hα emission stars that are significantly older than those TTSs associated with the BRCs. They apparently must have formed spontaneously before the main star formation event which gave birth to the massive stars in the region; however their origin is not clear. We found that in general WTTSs are older than CTTSs. It is also found that the fraction of CTTSs among the TTSs associated with the BRCs is found to decrease with age, as found in Taurus region by Armitage et al. (2003). These facts are in accordance with the conclusion by Bertout et al. (2007) that CTTSs evolve into WTTSs.

The CMF of 'A'-type BRCs seems to follow a MF similar to that found in young open clusters, whereas 'B/C'-type BRCs have a significant steeper CMF, indicating that BRCs of the latter type tend to form relatively more low-mass YSOs of the mass range $0.2 \leq M/\mathrm{M}_{\odot} \leq 0.8$.

ACKNOWLEDGMENTS

We are thankful to the anonymous referee for the critical comments which improved the scientific contents and presentation of the paper. We are thankful to the TAC and staff of *HCT* for the time allotment and for their support during the observations, respectively. This publication makes use of data from the 2MASS (a joint project of the University of Massachusetts and the Infrared Processing and Analysis Center/California Institute of Technology, funded by the National Aeronautics and Space Administration and the National Science Foundation), archival data obtained with the *Spitzer Space Telescope* (operated by the Jet Propulsion Laboratory, California Institute of Technology, under contract with the NASA). This study is a part of the DST (India) sponsored project and NC is thankful to DST for the support. NC also acknowledges the financial support provided by TIFR during her visit to TIFR. AKP and KO acknowledge the financial support received from DST (India) and JSPS (Japan).

REFERENCES

Allen L. E. et al., 2004, ApJS, 154, 363
Allen L. E., Hora J. L., Megeath S. T., Deutsch L. K., Fazio G. G., Chavarria L., Dell R. W., 2005, Int. Astron. Union Symp., 227, 352
Armitage P. J., Clarke C. J., Palla F., 2003, MNRAS, 342, 1139

Bertoldi F., 1989, ApJ, 346, 735
Bertout C., Siess L., Cabrit S., 2007, A&A, 473, L21
Bessell M. S., Brett J. M., 1988, PASP, 100, 1134
Caillault J. P., Brice no C., Mart'in E. L., Palla F., Wichmann R., 1998, in Donahue R. A., Bookbinder J. A., eds, ASP Conf. Ser. Vol. 154, Cool Stars, Stellar Systems and the Sun. Astron. Soc. Pac., San Fransisco, p. 237
Carpenter J. M., Heyer M. H., Snell R. L., 2000, ApJS, 130, 381
Cohen J. G., Frogel J. A., Persson S. E., Ellias J. H., 1981, ApJ, 249, 481
Contreras M. E., Sicilia-Aguilar A., Muzerolle J., Calvet N., Berlind P., Hartmann L., 2002, ApJ, 124, 1585
Cutri R. M. et al., 2003, Vizier Online Data Catalog, 2246, O
Dale J. E., Bonnell I. A., Whitworth A. P., 2007, MNRAS, 375, 1291
Deharveng L., Zavagno A., Cruz-Gonzalez I., Salas L., Caplan J., Carrasco L., 1997, A&A, 317, 459
Deharveng L., Zavagno A., Salas L., Porras A., Caplan J., Cruz-Gonzalez I., 2003, A&A, 399, 1135
De Vries C. H., Narayanan G., Snell R. L., 2002, ApJ, 577, 798
Edwards S., Hartigan P., Ghandour L., Andrulis C., 1994, AJ, 108, 1056
Elmegreen B. G., Lada C. J., 1977, ApJ, 214, 725
Elmegreen B. G., 1998, in Woodward C. E., Shull J. M., Thronson H. A., eds, ASP Conf. Ser. Vol. 148, Origins: Observations and Theory of Dynamical Triggers for Star Formation. Astron. Soc. Pac., San Fransisco, p. 150
Feinstein A., Vazquez R. A., Benvenuto O. G., 1986, A&A, 159, 223
Furlan E. et al., 2006, ApJ, 165, 568
Getman K. V., Feigelson E. D., Garmire G., Broos P., Wang J., 2007, ApJ, 654, 316
Girardi L., Bertelli G., Bressan A., Chiosi C., Groenewegen M. A. T., Marigo P., Salasnich B., Weiss A., 2002, A&A, 391, 195
Gras-Vel'azquez A., Ray T. P., 2005, A&A, 443, 541
Haisch K. E., Lada E. A., Lada C. J., 2001, AJ, 121, 2065
Hartmann L., 2001, AJ, 121, 1030
Hartmann L., 2003, ApJ, 585, 398
Hartmann L., Hewett R., Calvet N., 1994, ApJ, 426, 669
Herbst W., Assousa G. E., 1977, ApJ, 217, 473
Hillenbrand L. A., 2005, in Livio M., ed., A Decade of Discovery: Planets Around Other Stars STScI Symposium Series 19, astro-ph/0511083
Hillenbrand L. A., Strom S. E., Vrba F. J., Keene J., 1992, ApJ, 397, 613
Hosokawa T., Inutsuka S.-I., 2005, ApJ, 623, 917
Hosokawa T., Inutsuka S.-I., 2006, ApJ, 646, 240
Ikeda H. et al., 2008, AJ, 135, 2323
Johnstone D., Matsuyama I., McCarthy I. G., Font A. S., 2004, Rev. Mex. Astron. Astrofis, 22, 38
Jose J. et al., 2008, MNRAS, 384, 1675
Karr J. L., Martin P. G., 2003, ApJ, 595, 900
Kenyon S., Hartmann L., 1995, ApJS, 101, 117
Kessel-Deynet O., Burkert A., 2003, MNRAS, 338, 545
Koenig X. P., Allen L. E., Gutermuth R. A., Hora J. L., Brunt C. M., Muzerolle J., 2008, ApJ, 688, 1142
Kroupa P., 2001, MNRAS, 322, 231
Kroupa P., 2002, Sci, 295, 82
Landolt A. U., 1992, AJ, 104, 340
Lang K. R., 1992, Astrophysical Data: Planets and Stars. Springer-Verlag, New York, p. 132
Lawson W. A., Fiegelson E. D., Huenemoerder D. P., 1996, MNRAS, 280, 1071
Lefloch B., Lazareff B., 1994, A&A, 289, 559
Lefloch B., Lazareff B., 1995, A&A, 301, 522
Lefloch B., Lazareff B., Castets A., 1997, A&A, 324, 249
Manoj P., Bhatt H. C., Maheswar G., Muneer S., 2006, ApJ, 653, 657
Mart'in E. L., 1998, AJ, 115, 351
Matsuyanagi I., Itoh Y., Sugitani K., Oasa Y., Mukai T., Tamura M., 2006, PASJ, 58, L29
Megeath S. T. et al., 2004, ApJS, 154, 367
Meyer M., Calvet N., Hillenbrand L. A., 1997, AJ, 114, 288
Miao J., White G. J., Nelson R., Thompson M., Morgan L., 2006, MNRAS, 369, 143
Morgan L. K., Thompson M. A., Urquhart J. S., White G. J., Mio J., 2004, A&A, 426, 535
Morgan L. K., Thompson M. A., Urquhart J. S., White G. J., 2008, A&A, 477, 557
Muzerolle J., Calvet N., Hartmann L., 2001, ApJ, 550, 994
Nakano M., Sugitani K., Niwa T., Itoh Y., Watanabe M., 2008, PASJ, 60, 739
Ogura K., Sugitani K., Pickles A., 2002, AJ, 123, 2597
Ogura K., Chauhan N., Pandey A. K., Bhatt B. C., Ojha D. K., Itoh Y., 2007, PASJ, 59, 199 (Paper I)
Ojha D. K. et al., 2004a, ApJ, 608, 797
Ojha D. K. et al., 2004b, ApJ, 616, 1042
Pandey A. K., Sharma S., Ogura K., Ojha D. K., Chen W. P., Bhatt B. C., Ghosh S. K., 2008, MNRAS, 383, 1241
Patel N. A., Heyer M. H., Goldsmith P. F., Snell R. L., Hezel T., Pratap P., 1994, in Clemens D. P., Barvainis R., eds, ASP Conf. Ser. Vol. 65, Clouds, Cores, and Low-Mass Stars. Astron. Soc. Pac., San Fransisco, p. 81
Patel N. A., Goldsmith P. F., Heyer M. H., Snell R. L., Pratap P., 1998, ApJ, 507, 241
Reach W. et al., 2006, Infrared Array Camera Data Handbook, version 3.0. Spitzer Science Centre, Pasadena
Robitaille T. P., Whitney B. A., Indebetouw R., Wood K., Denzmore P., 2006, ApJS, 167, 256
Samal M. R., Pandey A. K., Ojha D. K., Ghosh S. K., Kulkarni V. K., Bhatt B. C., 2007, ApJ, 671, 555
Schaller G., Scherer D., Meynet G., Maeder A., 1992, A&AS, 96, 269
Sharma S., Pandey A. K., Ojha D. K., Chen W. P., Ghosh S. K., Bhatt B. C., Maheswar G., Sagar R., 2007, MNRAS, 380, 1141
Shevchenko V. S., Ezhkova O. V., Ibrahimov M. A., van den Ancker M. E., Tjin A Djie H. R. E., 1999, MNRAS, 310, 210
Sicilia-Aguilar A., Hartmann L. W., Briceno C., Muzerolle J., Calvet N., 2004, AJ, 128, 805
Sicilia-Aguilar A., Hartmann L. W., Harnandez J., Briceno C., Calvet N., 2005, AJ, 130, 188
Siess L., Dufour E., Forestini M., 2000, A&A, 358, 593
Stetson P. B., 1987, PASP, 99, 191
Sugitani K., Ogura K., 1994, ApJS, 92, 163
Sugitani K., Fukui Y., Ogura K., 1991, ApJS, 77, 59 (SFO91)
Sugitani K., Tamura M., Ogura K., 1995, ApJ, 455, L39
Sung H., Chun M. Y., Bessel M. S., 2000, AJ, 120, 333
Thompson M. A., White G. J., Morgan L. K., Miao J., Fridlund C. V. M., Huldtgren-White M., 2004, A&A, 414, 1017
Vallee V. P., Hughes V. A., Viner M. R., 1979, A&A, 80, 189
Walter F. M., Brown A., Matthieu R. D., Meyer P. C., Vrba F. J., 1988, AJ, 96, 297
Whitney B. A., Wood K., Bjorkman J. E., Cohen M., 2003, ApJ, 598, 1079
Yang J., Fukui Y., 1992, ApJ, 386, 618

SUPPORTING INFORMATION

Additional Supporting Information may be found in the online version of this article:

Table 6. IRAC photometric magnitudes of the disc-bearing candidates in BRCs 2, 27 and 13/14.
Table 7. *J*, *H* and *K* magnitudes of the sources used in the analysis (cf. Section 6.2).
Appendix A. Spatial distribution of YSOs in and around BRC regions.

Please note: Wiley-Blackwell are not responsible for the content or functionality of any supporting information supplied by the authors. Any queries (other than missing material) should be directed to the corresponding author for the article.

This paper has been typeset from a TEX/LATEX file prepared by the author.